Geometric, energetic, and bonding properties of neutral and charged copper-doped silicon clusters

Chuanyun Xiao* and Frank Hagelberg†
Computational Center for Molecular Structure and Interactions, Jackson State University, Jackson, Mississippi 39217

William A. Lester, Jr.
Kenneth S. Pitzer Center for Theoretical Chemistry, Department of Chemistry, University of California at Berkeley, Berkeley, California 94720-1460

(Received 2 January 2002; revised manuscript received 25 April 2002; published 30 August 2002)

The geometric, energetic, and bonding properties of $CuSi_n$ ($n=4$, 6, 8, 10, and 12) clusters in neutral and charged states are studied systematically using a hybrid density functional method (B3LYP). The Si_n frameworks in most isomers of $CuSi_n$ are found to adopt the geometries of the ground-state or low-lying isomers of Si_n or Si_{n+1}, with Cu at various substitutional or adsorption sites. Several cagelike structures with Cu at the center site are found for $CuSi_{10}$ and $CuSi_{12}$. A hexagonal double-chair structure with Cu at the center, which bears a similarity to the structure of a regular hexagonal prism recently reported for WSi_{12}^+ [H. Hiura *et al.*, Phys. Rev. Lett. **86**, 1733 (2001)], is identified as the best candidate for the ground state of $CuSi_{12}$. The Cu-Si bond in $CuSi_n$ is strong for the substitutional and the center-site structures, but weak for the adsorption structures where charge transfer and resulting ionic interaction is found to play a more important role. The Cu atom reveals a similar bonding character to the replaced Si atom in the substitutional structures except for $CuSi_{12}$, where the Cu atom both in the substitutional and in the center-site structures is found to form multicenter bonds with as many as nine (substitutional) to 12 (center-site) Si atoms. Various energetic properties, including binding and dissociation energies, ionization potentials, electron affinities, and vertical detachment energies are reported for $CuSi_n$.

DOI: 10.1103/PhysRevB.66.075425 PACS number(s): 31.15.Dv, 36.40.Cg, 61.46.+w, 73.22.−f

I. INTRODUCTION

Since the discovery and large-scale synthesis of C_{60}, fullerenes and metallofullerenes have been the focus of extensive investigations. These investigations indicated that the doped atoms can interact with the fullerenes in three possible ways: (1) encapsulated inside the fullerene cage (endohedral),[1] (2) adsorbed outside the fullerene cage (exohedral),[2] and (3) incorporated into the fullerene network by substitution of carbon atoms (substitutional).[3] The successful syntheses of heterofullerenes opened up the possibility of fine tuning the electronic properties of the cage structures via selected doping. It was found that doped atoms can dramatically modify the electronic properties of fullerenes in a variety of ways, leading to the discovery of unprecedented phenomena such as superconductivity, magnetism, and chemical reactivity, and that doped atoms can strongly stabilize some fullerenes that are otherwise unstable.[4]

Similar to fullerenes, intensive research was carried out in recent years on pure silicon clusters to understand the size dependence of their structures and properties.[5–10] These studies revealed that the geometric structures of small silicon clusters differ from those of carbon clusters. Cagelike structures of fullerenes have not been experimentally found for pure silicon clusters to date, to our knowledge.

In contrast to metallofullerenes, much fewer efforts have been devoted to metal-doped silicon clusters. The problem of the metal-silicon bond was a topic of a number of studies in bulk metal-silicon systems, both experimentally[11–13] and theoretically.[14–17] The motivation for the great and persisting interest in this topic consists of both its fundamental relevance to the understanding of the silicon-based composite materials and its high degree of practical importance in view of the ample use made of metal-doped silicon structures in microelectronic technology. It appears that the basic processes governing the interaction between a metal impurity and the silicon host can be studied more easily in a finite cluster than in an extended system, as a cluster is more easily accessible to accurate computational analysis than the surface or bulk systems. This consideration provides a strong motivation for the study of the mixed metal-silicon clusters. On the other hand, the hope to explore mixed silicon clusters with special properties for interesting material designs is another strong motivation for cluster study. For example, the possibility of stabilizing fullerenelike structures of silicon clusters by metal atoms is a topic of increasing interest.

Several experimental projects dealt with the metal-silicon systems. In the pioneering work of Beck,[18] the metal-silicon clusters MSi_n, with $M=$ Cu, Cr, Mo, and W, were generated using a laser vaporization technique. The mass spectrum of $CuSi_n$ ($6 \leqslant n \leqslant 12$) yielded exceptional stability for $CuSi_{10}$. More recently, Scherer and co-workers[19–21] produced small metal-silicon clusters M_mSi_n for three noble metal elements ($M=$Cu,Ag,Au) with $m>1$. Kishi *et al.*[22] carried out a combined experimental and theoretical study of $NaSi_n$ ($n \leqslant 7$), and found that the Na atom serves as an electron donor to the Si_n framework and that the most stable isomer of $NaSi_n$ retains the framework of the corresponding Si_n cluster nearly unchanged upon the adsorption of Na.

Very recently, the authors of Ref. 23 reported experimental evidence of the formation of stable metal-encapsulating Si cage cluster ions MSi_n^+ ($M=$ Hf, Ta, W, Re, Ir, etc., with $n=14$, 13, 12, 11, 9, respectively) and proposed a structural model of a regular hexagonal prism for WSi_{12} with the W atom at the center in an *ab initio* theoretical analysis. This finding arouses increasing interest in the search for cagelike

Si clusters stabilized by metal atoms.

Stimulated by the experimental findings, several computational investigations were performed for metal-doped silicon clusters.[24–30] Also, considerable efforts have been invested in the computational search for fullerenelike silicon clusters stabilized by metal atoms.[31,32] Very recently, Kumar and Kawazoe[33,34] reported theoretical findings of several types of metal-encapsulating caged structures with high stability for a series of $M@Si_n$ clusters ($n=14-17$, $M=$Cr, Mo, W, Fe, Ru, Os, Ti, Zr, Hf).

We have initiated a series of theoretical studies on the geometric and electronic properties of $CuSi_n$ clusters.[28–30] In two recent contributions,[28,29] we reported studies of the geometries and stabilities of neutral $CuSi_n$ ($n=4,6,8,10,12$) clusters using a hybrid density functional method (B3LYP). However, the emphasis of these investigations was on cluster geometries and stabilities, while a bonding analysis was carried out only for selected $CuSi_4$ and $CuSi_6$ isomers.[28] In addition, since most experimental measurements are performed on the charged species, the impact of charge on the structures and properties of clusters has to be explored.

In this paper, we extend our study of neutral $CuSi_n$ ($n=4,6,8,10,12$) clusters to the neutral and charged species and report results in the following aspects: (1) presenting some low-lying isomers and examining the influence of positive and negative charges on the structures and energetics of $CuSi_n$ clusters; (2) extending the bonding analysis for $CuSi_4$ and $CuSi_6$ to clusters up to $CuSi_{12}$, so as to gain a better understanding of the Cu-Si bonding in different types of structures; and (3) presenting our theoretical results of various energetic properties, including binding and dissociation energies, ionization potentials, electron affinities, and vertical detachment energies of $CuSi_n$ clusters. The paper is arranged as follows: the computational details are described in Sec. II; the results and discussion are presented in Sec. III, and our final conclusions are given in Sec. IV.

II. COMPUTATIONAL DETAILS

In previous studies of neutral $CuSi_n$ ($n=4,6,8,10,12$) clusters,[28,29] we employed the B3LYP hybrid density functional method with a basis set labeled GEN, which is a combination of the 6-31$G(d)$ basis set for Si and a $[8s,6p,4d,1f]$ basis set for Cu. The latter is taken from Wachter's $[8s,6p,2d]$ basis set[35] augmented by d and f polarization functions and is nearly equivalent to the 6-311$G(d)$ basis set. Since diffuse functions are important for proper description of anionic clusters, we chose, in the present study, the 6-311+$G(d)$ basis set for both Cu and Si and applied the B3LYP method as in our previous publications.

The quality of the B3LYP/6-311+$G(d)$ scheme for the description of Cu-Si clusters was tested by calculations on Si and Cu atoms and their dimers. As seen in Table I, the calculated bond lengths, binding energies, vibrational frequencies, adiabatic ionization potentials, and adiabatic electron affinities for Si and Cu atoms and their dimers in all charge states are in quite good agreement with available experimental data and other *ab initio* and density-functional calculations.[5,7,20,36–48] The B3LYP/6-311+$G(d)$ results are usually close to those of the B3LYP/GEN approach but reveal noticeable improvement in the electron affinities. For Si_2^+ and $CuSi^-$, no experimental data are available and our B3LYP/6-311+$G(d)$ results compare well with previous calculations.[37,41,45] In addition, we have checked the influence of increasing the number of polarization functions in the 6-311+$G(md,nf)$ basis set series ($m\leqslant 3, n\leqslant 2$) for Si and Cu atoms and their dimers as well as for the most stable isomer of $CuSi_4$ (**4a**), and found that the increase in the number of the polarization functions beyond 6-311+$G(d)$ has only a slight effect on the geometries [<0.01 Å in the bond lengths of $CuSi_4$ (**4a**)].

In the calculations performed previously at the B3LYP/GEN level, we[28,29] searched extensively for the low-lying isomers of $CuSi_n$ by placing a Cu atom at various adsorption or substitutional sites and the center of a number of selected Si frameworks: (1) Cu is placed at various adsorption sites and the center of the ground-state or low-lying isomers of Si_n as determined by *ab initio* and density-functional calculations (Fig. 1).[5–10] (2) Cu is placed at various adsorption sites and the center of highly symmetric cagelike structures of Si_n, and (3) Cu is placed at various substitutional sites of the ground-state or low-lying isomers of Si_{n+1} (Fig. 1).[5–10] These structures were subject to full geometry optimization at the B3LYP/GEN level. Note that these considerations of Cu-Si interactions correspond to the three types of metal-fullerene interactions in metallofullerenes.

Most of the geometries reported in this paper for neutral $CuSi_n$ clusters at the B3LYP/6-311+$G(d)$ level were derived by further relaxing the structures of neutral $CuSi_n$ at the B3LYP/GEN level. The relaxation is usually quite small. In addition, several low-lying isomers were found and reported in this paper for $CuSi_6$, $CuSi_8$, and especially $CuSi_{12}$ with above-mentioned search strategy. The influence of charge on the structures, stabilities and energetics of $CuSi_n$ clusters was then examined by relaxing all neutral isomers without any symmetry constraint in the singly cationic and anionic charge states.

We assumed a spin doublet state for all neutral and singlet state for all charged $CuSi_n$ isomers in the present calculation. The doublet states were shown to correspond to the ground state of neutral $CuSi_n$ species in our previous calculations.[28,29] A spin-unrestricted scheme was adopted for open-shell species, and the spin contamination was found to be negligible for all cases.

The stabilities of all stationary points were examined by vibrational analysis. In the case of an imaginary frequency, relaxation along the corresponding unstable normal coordinate was carried out until a true local minimum was reached.

The geometries for the ground and low-lying states of pure Si_n ($n=4-13$) clusters in the neutral and charged states were reoptimized at the B3LYP/6-311+$G(d)$ level; see Fig. 1 for comparison with the results of $CuSi_n$ clusters. All calculations were performed with the GAUSSIAN 94 package.[49]

III. RESULTS AND DISCUSSION

In the following, we will first describe the geometries and relative stabilities of individual Si_n ($n=4-13$) and $CuSi_n$

TABLE I. Comparison of calculated properties at B3LYP/6-311+$G(d)$ and B3LYP/GEN levels with experimental data and other *ab initio* and density-functional results for Si and Cu, atoms and their dimers. R_e: bond length (Å); E_b: binding energy (in eV); ω_e: vibrational frequency (in cm^{-1}); IP: ionization energy (in eV); EA: electron affinity (in eV).

		R_e	E_b	ω_e	*IP*	*EA*
Si	B3LYP/GEN				8.113	0.948
	B3LYP/6-311+$G(d)$				8.112	1.327
	QCISD(T)/(7s,6p,3d,1f)[a]					1.35
	$G2$[b]					1.355
	CASSCF/CASPT2+DK[c,†]				7.92	1.34
	Expt.				8.15[d]	1.385[e]
Cu	B3LYP/GEN				8.030	1.002
	B3LYP/6-311+$G(d)$				8.037	1.212
	LCGTO-LSD[f]				8.61	1.56
	CASSCF/CASPT2+DK[c,†]				7.82	0.83
	Expt.[f]				7.724	1.235±0.005
Si_2	B3LYP/GEN	2.286	3.081	490	7.905	1.815
	B3LYP/6-311+$G(d)$	2.280	3.065	487	7.919	2.091
	MP4/(6s,5p,3d,1f)[g]	2.265	3.06	507		
	QCISD(T)/(7s,6p,3d,1f)[a]					2.09
	$G2$		3.191[b,h]		7.944[h]	2.208[b]
	Expt.	2.246[i,j]	3.209[i]	509±10[j]	7.921[k]	2.176±0.002[j]
Cu_2	B3LYP/GEN	2.265	1.885	249	7.984	0.697
	B3LYP/6-611+$G(d)$	2.279	1.804	241	8.001	0.847
	LCGTO-LSD[f]	2.20	2.60	216	8.69	1.11
	LCGTO-GGA[f]	2.27	2.26	205	8.82	1.39
	Expt.[f]	2.22	2.08±0.02	265	7.904	0.836±0.006
CuSi	B3LYP/GEN	2.247	2.093	332	7.226	1.255
	B3LYP/6-311+$G(d)$	2.251	2.038	326	7.246	1.475
	MP2/6-311+$G(d)$[l]		1.783		6.874	1.325
	QCISD/6-311+$G(d)$[l]	2.242	1.830	336	6.744	1.222
	QCISD(T)/6-311+$G(d)$[l]	2.235	1.787[‡]	325	7.009[‡]	1.424[‡]
	CASSCF/CASPT2[c]	2.270	1.985	376	7.052	1.502
	CASSCF/CASPT2+DK[c,†]	2.199	2.192	384	7.106	1.520
	Expt.	2.28[m]	2.25,[m] 2.36[n]	320[m]		
Si_2^+	B3LYP/GEN	2.304	3.289	441		
	B3LYP/6-311+$G(d)$	2.302	3.258	435		
	MP2/6-31$G(d)$[h]	2.263				
Cu_2^+	B3LYP/GEN	2.423	1.932	179		
	B3LYP/6-311+$G(d)$	2.450	1.840	166		
	LCGTO-LSD[f]	2.34				
	LCGTO-GGA[f]	2.36				
	Expt.[f]			187±8		
$CuSi^+$	B3LYP/GEN	2.251	2.897	347		
	B3LYP/6-311+$G(d)$	2.255	2.828	340		
	B3LYP/6-311+$G(3df)$[o,§]		2.810			
	MP2/6-611+$G(d)$[l]		2.165			
	QCISD/6-611+$G(d)$[l]	2.257	2.270	358		
	QCISD(T)/6-311+$G(d)$[l]	2.258	2.158[‡]	311		
	$G2$[o]		2.710			
	CCSD(T)/6-311+$G(3df)$[o]		2.003[¶]			
	CASSCF/CASPT2[c]	2.194	3.836	372		
	CASSCF/CASPT2+DK[c,†]	2.152	3.039	371		
	Expt.[o]		2.650±0.078			

TABLE I. (*Continued.*)

		R_e	E_b	ω_e	*IP*	*EA*
Si_2^-	B3LYP/GEN	2.203	3.948	544		
	B3LYP/6-311+$G(d)$	2.198	3.830	537		
	MP2/6-31$G(d)$[a]	2.202				
	Expt.[j]	2.207±0.005		533±5		
Cu_2^-	B3LYP/GEN	2.393	1.581	187		
	B3LYP/6-311+$G(d)$	2.404	1.439	180		
	LCGTO-LSD[−f]	2.33		205		
	LCGTO-GGA[f]	2.44		183		
	Expt.	2.35±0.01[f,p]	1.57±0.06[p]	210±15[f,p]		
$CuSi^-$	B3LYP/GEN	2.279	2.400	295		
	B3LYP/6-311+$G(d)$	2.274	2.186	294		
	MP2/6-311+$G(d)$[l]		2.054			
	QCISD/6-311+$G(d)$[l]	2.262	2.036	283		
	QCISD(T)/6-311+$G(d)$[l]	2.268	2.034[‡]	270		
	CASCF/CASPT2[c]	2.164	3.015	299		
	CASSCF/CASPT2+DK[c,†]	2.154	3.037	384 (?)		

[a]Reference 7.
[b]Reference 36.
[c]Reference 37.
[d]Reference 38.
[e]Reference 39.
[f]Reference 40.
[g]Reference 5.
[h]Reference 41.
[i]Reference 42.
[j]Reference 43.
[k]Reference 44.
[l]Reference 45.
[m]Reference 20.
[n]Reference 46.
[o]Reference 47.
[p]Reference 48.
[†]DK means one-component relativistic Douglas-Kroll correction.
[‡]Single-point calculation with geometry optimized at QCISD/6-311+$G(d)$ level.
[§]Single-point calculation with geometry optimized at B3LYP/6-311$G(d)$ level (2.142 Å, obtained from the authors).
[¶]Single-point calculation with geometry optimized at MP2/6-31$G(d)$ level (2.002 Å, obtained from the authors).
[(?)]This datum is questionable since it is too far from the CASSCF/CASPT2 value and is the same as the one for CuSi neutral.

(n=4,6,8,10,12) clusters in the neutral and charged states, then discuss the size dependence of various energetic properties of $CuSi_n$, including binding and dissociation energies, ionization potentials, electron affinities, and detachment energies, and finally analyze the Cu-Si bonding in representative $CuSi_n$ species.

A. Geometries of the ground-state and low-lying isomers of pure Si_n

Before describing the geometries of $CuSi_n$, we summarize the geometries of the ground-state and low-lying isomers of pure Si_n (n=4–13) clusters that are closely related to the $CuSi_n$ structures. The structures of Si_n (n=4–13) clusters have been studied extensively by both *ab initio* and density-functional approaches[5–10] and were reoptimized at the B3LYP/6-311+$G(d)$ level (see Fig. 1). For a review, the reader is referred to Ref. 9.

Among the small Si_n clusters ($n \leqslant 13$), Si_4, Si_6, Si_7, and Si_{10} are found with enhanced stability in the mass spectrum. The ground state of Si_4 is a planar rhombus (D_{2h}) in the neutral, cationic and anionic states,[5,9] while the ground state of Si_5 is a compressed trigonal bipyramid (D_{3h}).[5,9]

Si_6 has three low-lying isomers very close in energy:[5,9] an edge- and a face-capped trigonal bipyramid (C_{2v}-I and C_{2v}-II) and a compressed octahedron (D_{4h}). The

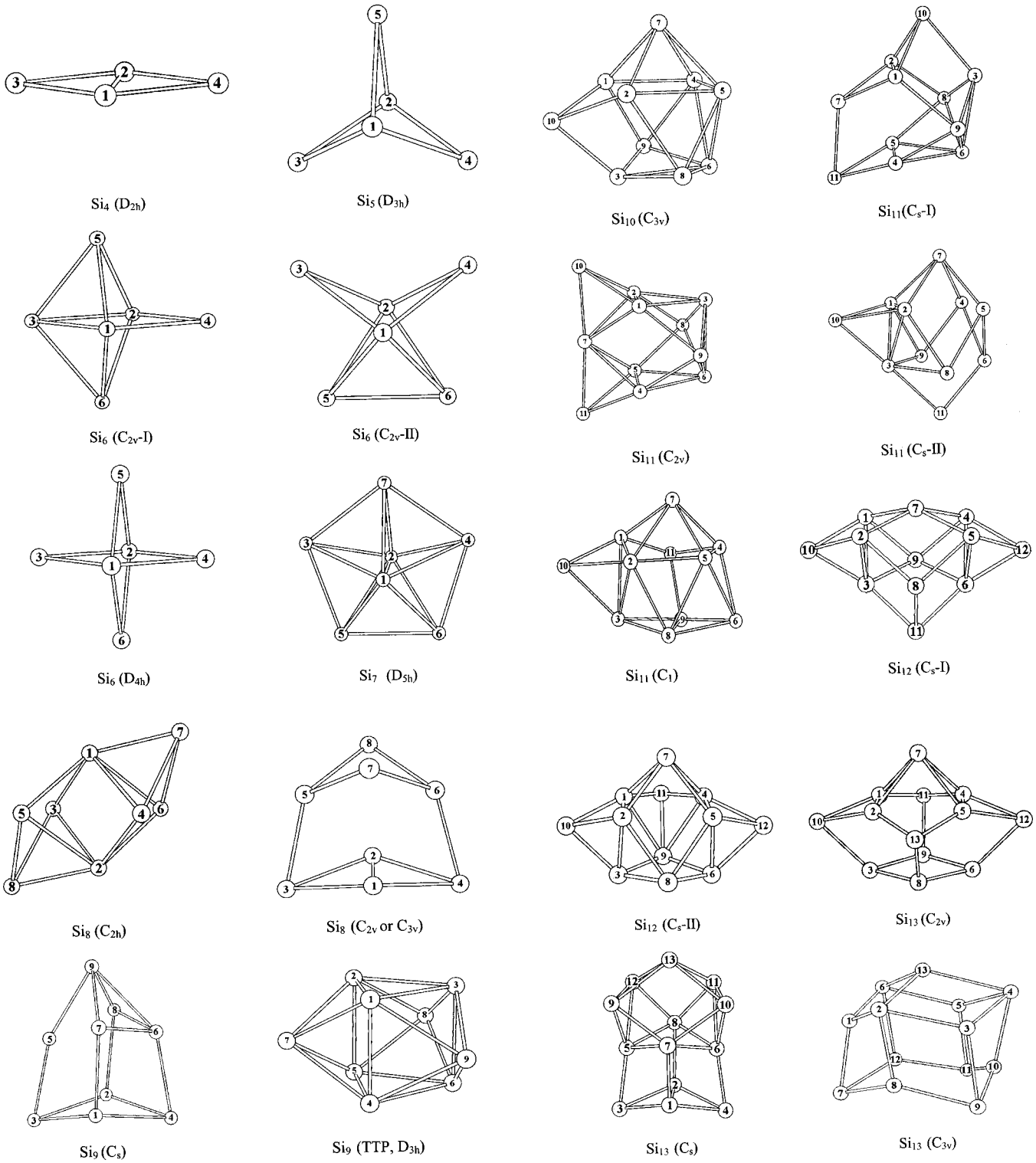

FIG. 1. Structures of Si_n clusters in the ground and low-lying states ($n=4-13$).

HF/6-31G calculation[5] favors the C_{2v}-I isomer over the C_{2v}-II and D_{4h} ones by 0.043 and 0.434 eV, respectively, while the PWB/DNP calculation[9] (using a gradient-corrected Perdew-Wang-Becke88 exchange-correlation functional and a double numerical plus polarization basis set in DMol) favors the D_{4h} isomer over the C_{2v}-I one (C_{2v}-II collapses to D_{4h}) by about 0.006 eV. At the B3LYP/6-311+$G(d)$ level, the C_{2v}-I isomer is the ground state while the C_{2v}-II and D_{4h} ones lie higher by 0.0007 and 0.035 eV, respectively. The C_{2v}-I structure remains the ground state of Si_6^+, while the C_{2v}-II structure becomes the ground state of Si_6^- which has a dihedral angle of 151.77° between the 3Si-1Si-2Si and 1Si-2Si-4Si faces (denoted as 3Si-1Si-2Si-4Si) that is much larger than the corresponding angle of neutral Si_6 (115.03°).

The ground state of neutral Si_7 is a pentagonal bipyramid (D_{5h}),[6,9] which corresponds to the Si_6 (C_{2v}-*II*) framework capped with a Si atom over the 3Si-4Si bridge. The geometric parameters of Si_7 (D_{5h}) are much closer to anionic Si_6^- (C_{2v}-*II*) than to neutral Si_6 (C_{2v}-*II*). For example, the 3Si-5Si bond length and the 3Si-5Si-6Si angle in neutral Si_6 (C_{2v}-*II*) are 2.72 Å and 99.13°, while the equivalent data in Si_6^- (C_{2v}-*II*) are 2.50 Å and 108.96°. The latter are very close to the respective values of 2.51 Å and 108.0° in Si_7 (D_{5h}). In fact, there is also a correspondence between the ground-state structures of Si_9 (C_s) and Si_8^- (C_{2v} or C_{3v}), Si_{11} (C_s-*I*), and Si_{10}^- (C_{3v}) as well as Si_{13} (C_{2v}) and Si_{12}^- (C_s-*II*).

The ground state of neutral Si_8 is a distorted bicapped octahedron (C_{2h}).[6,9] In addition, Si_8 has two low-lying isomers (C_{2v} and C_{3v}) (Ref. 9) which are similar in structure and are higher than Si_8 (C_{2h}) by 0.20 and 0.56 eV, respectively, at the B3LYP/6-311+$G(d)$ level. The C_{2v} and C_{3v} (7Si-2Si forming the trigonal axis shown in Fig. 1) isomers can both be viewed as a nearly planar rhombus interacting face to face with another bent rhombus. The C_{2h} geometry remains the ground state of Si_8^+, while the C_{2v} and C_{3v} isomers become competitive candidates for the ground state of Si_8^-.

The ground state proposed for neutral Si_9 is of C_{2v} symmetry at the PWB/DNP level,[9] which corresponds to the ground-state structure of anionic Si_8^- (C_{2v}) capped with a Si atom over the 7Si-8Si bridge. At the B3LYP/6-311+$G(d)$ level, this geometry will undergo a slight relaxation to a C_s symmetry (Fig. 1) with a minute energy gain of 0.01 eV. In addition, Si_9 has an important isomer with the shape of a tricapped trigonal prism (TTP,D_{3h}), which lies higher than Si_9 (C_s) by 1.49 eV at the B3LYP/6-311+$G(d)$ level, and has been shown to be a building block in many structures of larger Si_n clusters.[9] The C_s isomer remains the ground state of Si_9^+ while the ground state of Si_9^- is a slightly relaxed TTP structure (C_s symmetry).[9] The ground states and several low-lying isomers of Si_{10}, Si_{11}, Si_{12} and Si_{13} (Fig. 1) can all be built from the Si_9 (TTP,D_{3h}) structure by capping additional atoms on various faces.[6–10]

The ground states of Si_{10} and Si_{10}^- are both a tetracapped trigonal prism (C_{3v}), while the ground state of Si_{10}^+ undergoes a slight relaxation to a C_s symmetry from the C_{3v} geometry.[9] Among the four low-lying isomers of Si_{11}, the C_s-*I*, C_s-*II* (**11a** in Ref. 15) and C_1 (**11b** in Ref. 15) isomers all maintain the Si_{10} (C_{3v}) framework nearly unchanged. At the B3LYP/6-311+$G(d)$ level, the C_s-*I* isomer corresponds to the ground state of Si_{11}, while the C_{2v}, C_s-*II* and C_1 isomers are higher by 0.09, 0.23 and 0.30 eV, respectively. Calculations at the PWB/DNP (Ref. 9) and LDA (Ref. 8) (local density approximation) levels give the same energy ordering as that proposed by us for these isomers. In the PWB/DNP calculation,[9] where the C_s-*I*, C_s-*II* and C_{2v} isomers are denoted by $C_s(I)$, $C_s(II)$ and $C_{2v}(I)$, the C_{2v} and C_s-*II* isomers are higher than the C_s-*I* one by 0.022 and 0.297 eV, respectively, while in the LDA calculation[8] the C_1 isomer is higher than the C_s-*II* one by 0.132 eV.

The ground state of Si_{12} has a C_{2v} symmetry at the PWB/DNP level,[9] which corresponds to the Si_{11} (C_s-*II*) structure capped with an extra Si atom on the 4Si-5Si-6Si face. At the B3LYP/6-311+$G(d)$ level, however, such a configuration is a transition state and relaxation leads to two isomers, C_s-*I* and C_s-*II*, with the former lower than the latter by 0.49 eV. The C_s-*I* isomer is the ground state of Si_{12} and Si_{12}^+, while the C_s-*II* structure is the ground state of Si_{12}^-.

Further capping the 2Si-5Si-8Si face of Si_{12} (C_s-*II*) leads to Si_{13} (C_{2v}). This isomer was found by Rata *et al.*[10] [denoted therein as $C_{2v}(II)$]as the newest candidate for the ground state of Si_{13}^+, which is lower than the earlier proposed ground state for Si_{13}^+ (C_{2v} isomer in Ref. 9) by 0.39 eV at the PWB/DNP level, and we relaxed it for the neutral. In addition, Si_{13} has two other low-lying isomers (C_s and C_{3v}) that cannot be built from Si_9 (TTP). The C_s isomer was proposed as the ground state of Si_{13} in the PWB/DNP calculation[9] and it can be regarded as grown from a Si_8 (C_{2v}) unit. The C_{3v} isomer is a top-capped double-chair structure, reminiscent of the bulklike chair structure of Si_6 (D_{3d}) discussed in Ref. 11, and it is higher than the C_s isomer by 0.13 eV at the PWB/DNP level.[9] At the B3LYP/6-311+$G(d)$ level, the C_{2v} isomer corresponds to the ground state of neutral Si_{13} while the C_s and C_{3v} isomers are higher by 0.31 and 0.49 eV, respectively.

B. Geometries and relative stabilities of $CuSi_n$

Based on the ground-state and low-lying structures of Si_n described above, as well as the possible highly symmetric cagelike structures of Si_n, and using the optimization strategy described in Sec. II, we have conducted an extensive search for the low-lying isomers of $CuSi_n$ (n = 4,6,8,10,12). In total, three isomers for $CuSi_4$ and $CuSi_6$, nine isomers for $CuSi_8$, 20 isomers for $CuSi_{10}$, and 12 isomers for $CuSi_{12}$ have been found.

Since the experimental observations correspond to the most stable isomers, we will focus for each $CuSi_n$ species on the structures and properties of the isomers nearly isoenergetic with the most stable one (within 0.1 eV) and of some selected isomers of special interest to our discussion while the remaining isomers will be described only briefly. The optimized geometries for the selected $CuSi_n$ clusters are presented in Fig. 2, and related properties are listed in Tables III–VI and shown in Figs. 3–7. Optimized geometric parameters are given in Table II only for the most stable isomer of $CuSi_n$. The results for other isomers are available from the authors upon request. The isomers for selected neutral $CuSi_n$ are labeled as **na**, **nb**,... according to their energy ordering, while the corresponding isomers for $CuSi_n^+$ and $CuSi_n^-$ are labeled as **na**$^+$, **nb**$^+$,… and **na**$^-$, **nb**$^-$,…, respectively.

$CuSi_4$

Among the three isomers we identified for $CuSi_4$ (**4a**, **4b**, **4c**), the framework of a planar Si_4 (D_{2h}) rhombus is nearly retained in **4a** and **4b** with Cu at a face and an off-plane edge adsorption position, respectively (Fig. 2). Isomers **4b** and **4c** are obtained by the substitution of Cu for a Si atom at the

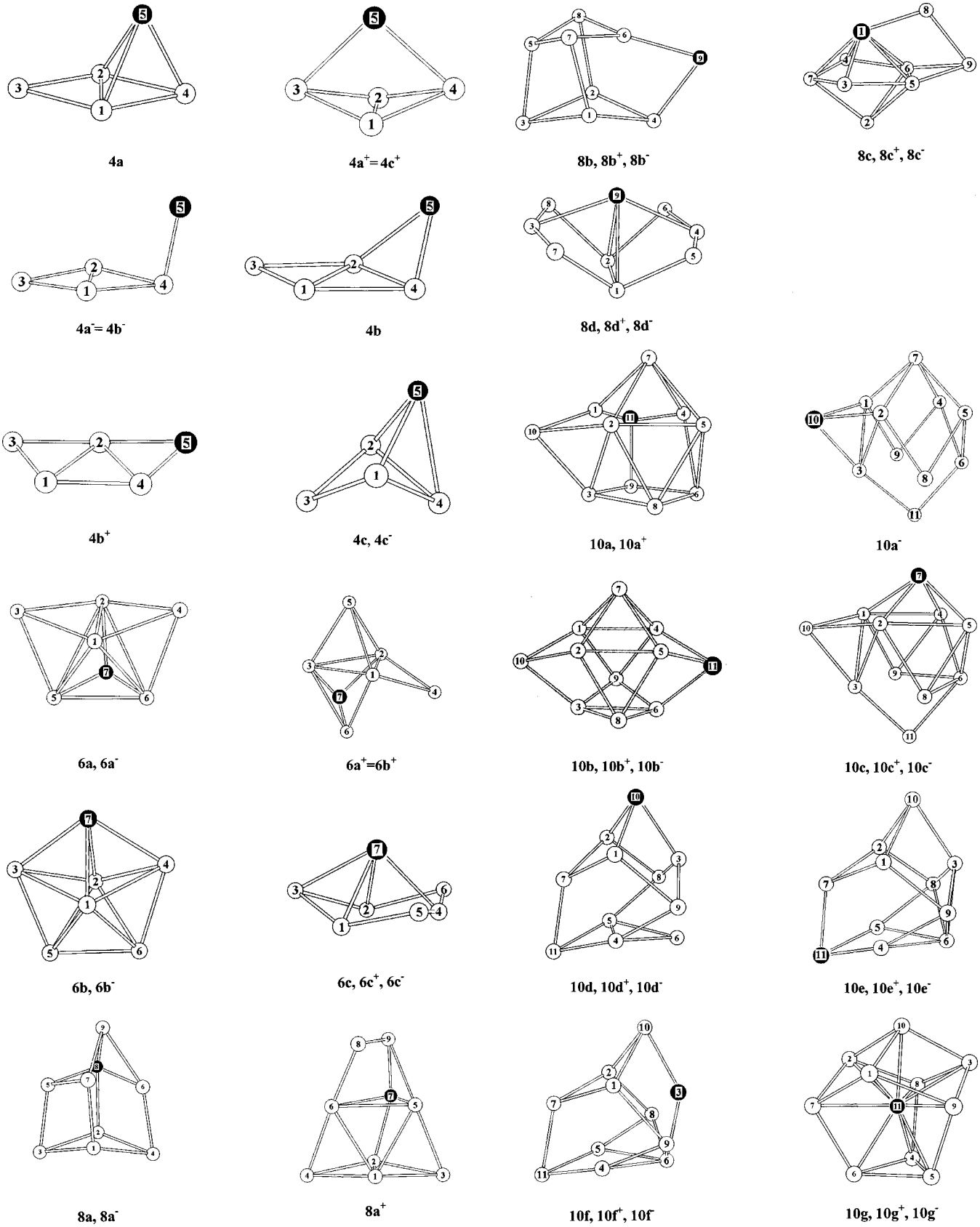

FIG. 2. Structures of selected $CuSi_n$ clusters in neutral and charged forms ($n=4-12$).

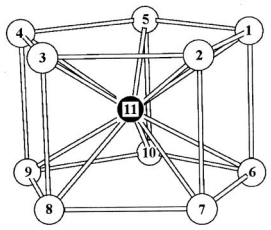

10h, 10h$^+$, 10h$^-$

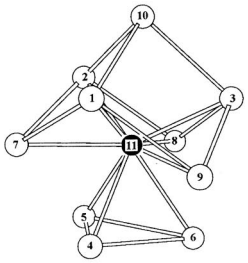

10i, 10i$^+$, 10i$^-$

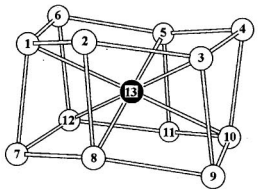

12a, 12a$^+$, 12a$^-$

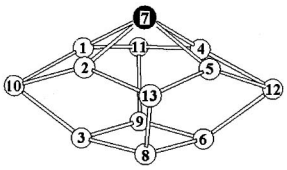

12b, 12b$^+$, 12b$^-$

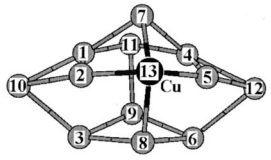

12c, 12c$^+$, 12c$^-$

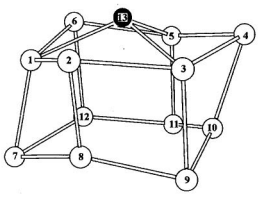

12d, 12d$^+$, 12d$^-$

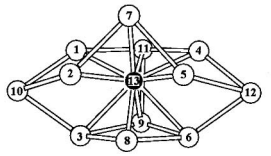

12e, 12e$^+$, 12e$^-$

FIG. 2. (*Continued.*)

apex or the equatorial site of Si_5 (D_{3h}), respectively. For all three isomers, symmetric adsorption, i.e., the top adsorption of Cu over the midpoint of planar Si_4 rhombus in **4a**, the coplanar adsorption of Cu on the 2Si-4Si edge of the planar Si_4 rhombus in **4b**, and the top adsorption of Cu over the midpoint of the 1Si-2Si bridge of the bent Si_4 rhombus in **4c**, turn out to be first-order transition states, which lie higher than the corresponding local minima only by 0.04–0.06 eV.

The three structures for neutral $CuSi_4$ species reduce to two different structures both in the cationic (**4a**$^+$ = **4c**$^+$,**4b**$^+$) and in the anionic (**4a**$^-$ = **4b**$^-$,**4c**$^-$) charge states (Fig. 2 and Table III). For the cationic species, the symmetric top adsorption and coplanar edge adsorption configurations, which are the transition states for neutral **4a** and **4b**, become the local minima for **4a**$^+$ (Fig. 2) and **4b**$^+$, respectively. For the anionic species, **4a**$^-$ = **4b**$^-$ can be described as an apex adsorption of Cu on the 4Si atom of a nearly planar Si_4 rhombus, while **4c**$^-$ maintains the framework of neutral **4c** nearly unchanged.

The relative energies of these species are listed in Table III. For the neutral species, the three isomers are nearly isoenergetic. For the cationic and anionic species, however, the two isomers are separated in energy by as much as 0.373 and 0.156 eV, respectively, and are, therefore, energetically distinguishable. For the cationic species, the energy order of **4a**$^+$ and **4b**$^+$ changes as compared to the neutral species. Because both the geometries and the relative stabilities of the neutral species are considerably different from the charged ones, any attempt to explain experimental results obtained for the charged species—such as mass spectroscopy, photoelectron spectroscopy, and ion mobility data—on the basis of the structures of the neutral clusters, is not justified.

$CuSi_6$

Among the three isomers identified for $CuSi_6$, **6a** corresponds to a face adsorption of Cu on the Si_6 (C_{2v}-*II*) framework while **6b** can be considered either as a top adsorption of Cu over Si_6 (C_{2v}-*II*) or an a substitutional structure of Si_7 (D_{5h}) with Cu at the equatorial 7Si site (Fig. 2). Similar to Si_7 (D_{5h}), the Si_6 framework in both **6a** and **6b** can be much more readily related to anionic Si_6^- (C_{2v}-*II*) than to neutral Si_6 (C_{2v}-*II*). To be specific, the 3Si-5Si bond length and the 3Si-5Si-6Si angle are 2.48 Å and 110.05° in **6a** (see Table II), and 2.48 Å and 108.78° in **6b**, which are much closer to the corresponding parameters in Si_6^- (C_{2v}-*II*) (2.50 Å and 108.96°) than in neutral Si_6 (C_{2v}-*II*) (2.72 Å and 99.13°). A substitutional structure similar to the present **6b** was reported by Kishi *et al.*[22] as the ground state of $NaSi_6$.

The last isomer **6c** represents the top adsorption of Cu above a hexagonal chair structure of Si_6 (D_{3d}).[5] This isomer is of interest since the chairlike framework of Si_6 is a fragment of bulk Si lattice and can be considered to be a finite counterpart of bulk Si.

It is worth pointing out that the substitutional isomer **6b** can be obtained either by substituting Cu for one of the equatorial atoms of Si_7 (D_{5h}) or by inserting Cu at the center of a regular (O_h) or compressed (D_{4h}) octahedron of Si_6. In the latter two cases, the Cu atom does not remain stationary at the center of the cage but moves to the surface, and the Si_6 (O_h or D_{4h}) framework relaxes into the ground-state structure of Si_6^- (C_{2v}-*II*). This indicates that a cagelike structure with Cu at the center site is not favored for $CuSi_6$. The reason is that the Si_6 (O_h or D_{4h}) cage is too small to enclose a Cu atom at the center without significantly weakening the Si-Si ligand interaction.

The three structures for neutral $CuSi_6$ are largely retained in the anionic charge state but will reduce to two (**6a**$^+$ = **6b**$^+$ and **6c**$^+$) structures in the cationic form (Fig. 2). The **6a**$^+$ = **6b**$^+$ structure corresponds to a face adsorption of Cu on Si_6 (C_{2v}-*I*) (Fig. 1), whereas **6c**$^+$ adopts a structure similar to neutral **6c**.

From Table III, one finds that **6a** and **6b** are competitive candidates for the ground state of $CuSi_6$, and represent an adsorption and a substitutional structure, respectively, in all charge states. The bulklike isomer **6c** is considerably higher than **6a** or **6b**, especially in the neutral and cationic charge states, indicating that the bulklike structure is unfavorable for $CuSi_6$. Note that the framework of Si_6 in **6a** and **6b** changes from Si_6 (C_{2v}-*II*) in the neutral and anionic species to Si_6

TABLE II. Optimized geometries (Å and degrees) for the most stable isomers of $CuSi_n$ (**4a**, **6a**, **8a**, **10a**, **12a**) at the B3LYP/6-311+$G(d)$ level. The dihedral angle between the *A-B-C* and *B-C-D* planes is denoted by *A-B-C-D*.

Cluster	Symmetry	Geometric parameter	Optimized value	Geometric parameter	Optimized value
$CuSi_4$	C_s	Cu-1Si	2.5635	1Si-3Si	2.3544
		Cu-4Si	2.3602	1Si-4Si	2.4047
		1Si-2Si	2.4376	3Si-1Si-2Si-4Si	179.6078
$CuSi_6$	C_s	Cu-2Si	2.3508	2Si-3Si	2.4506
		Cu-5Si	2.4421	2Si-5Si	2.8876
		1Si-2Si	2.4779	5Si-3Si	2.4764
		1Si-3Si	2.4106	5Si-6Si	2.4446
		2Si-5Si	2.4807	3Si-5Si-6Si	110.0478
$CuSi_8$	C_1	Cu-2Si	2.3635	2Si-3Si	2.3963
		Cu-5Si	2.4762	2Si-4Si	2.4114
		Cu-6Si	2.4541	3Si-5Si	2.4652
		Cu-7Si	3.8128	4Si-6Si	2.4090
		Cu-9Si	2.4563	7Si-5Si	2.4485
		1Si-2Si	2.6317	7Si-6Si	2.6875
		1Si-3Si	3595	9Si-5Si	2.6517
		1Si-4Si	2.4140	9Si-6Si	2.3919
		1Si-7Si	2.5712	9Si-7Si	2.4511
$CuSi_{10}$	C_1	Cu-1Si	2.4307	7Si-5Si	2.5360
		Cu-4Si	2.4146	2Si-5Si	2.5191
		Cu-7Si	3.8786	3Si-1Si	2.6158
		Cu-9Si	2.3347	3Si-2Si	2.5920
		10Si-1Si	2.4075	3Si-8Si	2.4369
		10Si-2Si	2.4182	3Si-9Si	2.3787
		10Si-3Si	2.3721	6Si-4Si	2.4804
		7Si-1Si	2.4694	6Si-5Si	2.5736
		7Si-2Si	2.5153	6Si-8Si	2.4996
		7Si-4Si	2.4690	6Si-9Si	2.4379
$CuSi_{12}$	C_{2h}	Cu-1Si	2.4464	2Si-3Si	2.4543
		Cu-2Si	2.9524	3Si-4Si	2.4130
		Cu-3Si	2.4565	1Si-7Si	2.3756
		Cu-4Si	2.7766	2Si-8Si	2.3902
		1Si-2Si	2.4468		

(C_{2v}-*I*) in the cationic species. This transformation is related to the change in the charge of the Si_6 framework in **6a** and **6b** in different charge states. Natural population analysis (NPA) (Table V) indicates that the Si_6 framework has a negative charge in both the neutral and the anionic species of **6a** and **6b** ($-0.52e$ and $-0.64e$ for **6a** and **6b** and -1.36 and -1.58 for $\mathbf{6a}^-$ and $\mathbf{6b}^-$). Therefore, the Si_6 framework in both the neutral and the anionic species of **6a** and **6b** corresponds to Si_6^- (C_{2v}-*II*), which is the ground state for Si_6^-. In contrast, the Si_6 framework in $\mathbf{6a}^+ = \mathbf{6b}^+$ possesses a positive charge ($+0.35e$), and hence tends to rearrange to the ground state Si_6^+ (C_{2v}-*I*) structure.

As a general observation, we have found that the Cu atom adopts a positive charge in all $CuSi_n$ ($n=4,6,8,10,12$) isomers investigated, and its charge changes only slightly with different charge states and sizes of the cluster. Typically, the charge of Cu in $CuSi_n$ is around $(0.50-0.60)e$ in the neutral and the anionic species, and $(0.30-0.40)e$ in the cationic species. As a representative case, the natural charges for atoms of **6a** in different charge states are indicated in Table V. Therefore, the Si_n framework exhibits a negative charge in all the neutral and the anionic species, and a positive charge in all the cationic species of $CuSi_n$. This leads to the finding that, as is the case for $CuSi_6$, most of the anionic isomers adopt structures similar to the corresponding neutral species while more cationic isomers are found with structures differing from their neutral counterparts.

$CuSi_8$

Four (**8a**–**8d**) of the nine isomers identified for $CuSi_8$ are shown in Fig. 2. Isomers **8a** and **8b** are a substitutional structure of Si_9 (C_s), with Cu occupying the 8Si site, and an adsorption structure of Si_8 (C_{2v}) with Cu capped over the 4Si-6Si bridge, respectively.

The other two isomers **8c** and **8d** are obtained by inserting Cu at the center of Si_8 (C_{2h}) or Si_8 (C_{2v}), respectively.

TABLE III. Relative energy ΔE (in eV), binding energy per atom E_b (in eV/atom), and dissociation energy D_e (in eV) for selected neutral and charged $CuSi_n$ species ($n=4,6,8,10,12$). For their definitions, see the text.

Cluster		Neutral			Cation			Anion		
		ΔE	E_b	D_e	ΔE	E_b	D_e	ΔE	E_b	D_e
$CuSi_4$	**4a**	**0.000**	2.466	1.453	0.000	2.680	2.523	**0.000**	2.674	1.715
	4b	0.003	2.466	1.450	**−0.373**	2.755	2.896		$\rightarrow$**4a**$^-$	
	4c	0.086	2.449	1.367		$\rightarrow$**4a**$^+$		0.156	2.643	1.559
$CuSi_6$	**6a**	**0.000**	2.805	1.637	**0.000**	2.999	2.993	0.000	2.945	1.737
	6b	0.078	2.794	1.559		$\rightarrow$**6a**$^+$		**−0.005**	2.946	1.742
	6c	0.913	2.674	0.724	1.179	2.830	1.815	0.126	2.927	1.612
$CuSi_8$	**8a**	**0.000**	2.888	1.999	**0.000**	3.044	3.400	**0.000**	3.067	2.119
	8b	0.008	2.887	1.991	0.038	3.040	3.363	0.084	3.077	2.202
	8c	0.357	2.849	1.642	0.258	3.015	3.142	0.401	3.023	1.718
	8d	0.949	2.783	1.050	0.542	2.984	2.858	0.615	2.999	1.504
$CuSi_{10}$	**10a**	**0.000**	3.009	1.356	0.000	3.178	3.210	0.000	3.157	1.951
	10b	0.006	3.008	1.350	0.229	3.157	2.981	−0.008	3.157	1.959
	10c	0.049	3.005	1.307	0.048	3.173	3.162	0.180	3.140	1.771
	10d	0.090	3.001	1.267	0.127	3.166	3.083	0.190	3.139	1.761
	10e	0.091	3.001	1.265	**−0.069**	3.184	3.280	0.422	3.118	1.529
	10f	0.289	2.983	1.068	0.494	3.133	2.716	**−0.077**	3.164	2.027
	10g	0.392	2.973	0.964	0.579	3.125	2.631	0.588	3.103	1.363
	10h	0.405	2.972	0.951	0.925	3.093	2.850	0.528	3.109	1.423
	10i	0.422	2.905	0.208	0.755	3.109	2.455	0.657	3.969	1.294
$CuSi_{12}$	**12a**	**0.000**	3.060	2.051	0.000	3.166	3.433	**0.000**	3.202	2.733
	12b	0.275	3.039	1.775	**−0.244**	3.185	3.677	0.500	3.164	2.233
	12c	0.342	3.034	1.708	−0.207	3.182	3.640	0.603	3.156	2.129
	12d	0.353	3.033	1.698	0.354	3.139	3.079	0.060	3.197	2.672
	12e	0.855	2.994	1.196	0.441	3.132	2.992	0.950	3.129	1.782

Strong relaxation occurs in **8c** and **8d**, and the Cu atom moves from the center to the surface, which is similar to the observation made for $CuSi_6$ and indicates that the surface-site structure is preferred over the center-site structure both for $CuSi_6$ and for $CuSi_8$.

In addition to **8a**, three other substitutional structures of Si_9 (C_s) are identified with Cu at the 4Si, 6Si, or 9Si sites, respectively, which are higher than **8a** by 0.36–0.50 eV. The substitution of Cu for 7Si in Si_9 (TTP, D_{3h}) and the top adsorption of Cu over Si_8 (C_{2v}) leads to two other isomers with energies higher than **8a** by around 0.26 eV, but the framework of these isomers reconstructs considerably. These five isomers are not shown in Fig. 2.

We note that **8a** can be obtained from several different initial geometries: It can be derived from substitution of Cu for 8Si in Si_9 (C_s) or for 1Si in Si_9 (D_{3h}), or from the insertion of Cu either at the center of Si_8 (C_{2v}) or the center of tetrahedral cage of Si_8. Similar to $CuSi_6$, the Cu atom in the latter two cases is found to be unstable in the center position and moves to the surface while the framework of Si_8 relaxes into that of Si_9 (C_s).

All of the above results document that the cagelike structure with Cu at the center site is unfavorable both for $CuSi_6$ and for $CuSi_8$. Alternatively, isomer **8d** bears similarity with the chair structure of **6c** with two more atoms (7Si and 8Si) capped on the 1Si-3Si and 2Si-3Si edges (Fig. 2). Just like $CuSi_6$, **8d** is also much higher than the most stable isomer **8a**, by 0.95 eV (Table II), suggesting that the bulklike structure is preferred neither for $CuSi_6$ nor $CuSi_8$.

The investigated charged $CuSi_8$ clusters nearly maintain the structures of the neutral species for all four isomers (**8a**–**8d**) in anionic form, and for **8b**$^+$, **8c**$^+$, and **8d**$^+$ in cationic form, while **8a**$^+$ is relaxed to a structure of **6a** capped with an 8Si-9Si dimer on the 5Si-6Si-Cu face. In fact, the structure of neutral **8a** can be related to another isomer of $CuSi_6$: it can be viewed as the structure of **6b** bicapped with 3Si and 4Si. As will be shown in Sec. III D, this connection leads to a notable similarity in the bonding properties of $CuSi_6$ and $CuSi_8$. From Table III, we find that **8a** and **8b** are competitive candidates for the ground state of $CuSi_8$ in all charge states.

$CuSi_{10}$

$CuSi_{10}$ is the cluster that occurs with the highest abundance in the mass spectrum.[18] Accordingly, the largest number of isomers has been identified for $CuSi_{10}$ among the $CuSi_n$ ($n=4,6,8,10,12$) series in our extensive search, and most of them represent substitutional structures.

In total, twenty isomers have been found for $CuSi_{10}$ and nine of them (**10a**–**10i**) are shown in Fig. 2. The structures of these twenty isomers can be classified into three types: two adsorption structures, 15 substitutional structures (with three also belonging to the adsorption type), and three center-

TABLE IV. Adiabatic ionization potential (AIP, in eV) and electron affinity (AEA, in eV) for selected neutral $CuSi_n$ species as well as vertical detachment energy (VDE, in eV) for corresponding anionic $CuSi_n^-$ species ($n=4,6,8,10,12$).

Cluster		AIP	AEA	VDE	VDE − AEA
$CuSi_4$	**4a**	6.968	2.365	2.591	0.226
	4b	6.592	2.368	2.591	0.223
	4c	6.882	2.295	2.791	0.496
$CuSi_6$	**6a**	6.680	2.308	2.606	0.298
	6b	6.603	2.391	2.513	0.122
	6c	6.947	3.095	3.509	0.414
$CuSi_8$	**8a**	6.636	2.940	3.183	0.243
	8b	6.666	3.031	3.352	0.321
	8c	6.537	2.896	3.128	0.232
	8d	6.229	3.274	3.564	0.290
$CuSi_{10}$	**10a**	6.183	2.950	3.550	0.600
	10b	6.407	2.964	3.211	0.247
	10c	6.182	2.819	3.169	0.350
	10d	6.220	2.850	3.074	0.224
	10e	6.022	2.620	2.921	0.301
	10f	6.388	3.316	3.478	0.162
	10g	6.370	2.754	3.304	0.550
	10h	6.703	2.828	2.919	0.091
	10i	6.516	2.715	2.961	0.246
$CuSi_{12}$	**12a**	6.590	3.175	3.352	0.177
	12b	6.136	2.950	3.179	0.229
	12c	6.105	2.915	3.279	0.364
	12d	6.654	3.468	3.645	0.177
	12e	6.240	3.080	3.306	0.226

TABLE VI. Natural electronic configuration for Cu and Na atoms in selected isomers of $CuSi_n$ and $NaSi_6$ cluster ($n=4,6,8,10,12$).

Cluster		Natural electronic configuration
$CuSi_4$	**4a**	Cu $3d^{9.90}4s^{0.58}4p^{0.04}4d^{0.01}$
	4b	Cu $3d^{9.91}4s^{0.58}4p^{0.03}$
	4c	Cu $3d^{9.88}4s^{0.55}4p^{0.05}4d^{0.01}$
$CuSi_6$	**6a**	Cu $3d^{9.89}4s^{0.55}4p^{0.03}$
	6b	Cu $3d^{9.89}4s^{0.41}4p^{0.05}$
$NaSi_6$		Na $3s^{0.09}3p^{0.01}$
$CuSi_8$	**8a**	Cu $3d^{9.86}4s^{0.51}4p^{0.05}4d^{0.01}$
	8b	Cu $3d^{9.91}4s^{0.55}4p^{0.02}$
$CuSi_{10}$	**10a**	Cu $3d^{9.90}4s^{0.45}4p^{0.02}4d^{0.01}$
	10b	Cu $3d^{9.90}4s^{0.58}4p^{0.02}5s^{0.01}$
	10c	Cu $3d^{9.87}4s^{0.50}4p^{0.05}4d^{0.01}$
	10g	Cu $3d^{9.87}4s^{0.52}4p^{0.25}4d^{0.06}5s^{0.01}$
$CuSi_{12}$	**12a**	Cu $3d^{9.87}4s^{0.42}4p^{0.16}4d^{0.05}5s^{0.02}$
	12d	Cu $3d^{9.88}4s^{0.42}4p^{0.07}4d^{0.02}5p^{0.01}$

site structures. Elements of the first two classes have been found in the smaller $CuSi_n$ clusters ($n=4,6,8$), in which the Cu atom always stays at a surface (adsorption or substitutional) site. However, no endohedral (center-site) structures with Cu occupying the center of a cagelike Si framework have so far been found stable for $CuSi_4$, $CuSi_6$, and $CuSi_8$.

Isomers **10a**–**10e** are the five competitive candidates for the ground state of $CuSi_{10}$ (Fig. 2 and Table III). Isomer **10b** is an adsorption structure of Si_{10} (C_{3v}), **10c** and **10d** are

TABLE V. Natural charges for all atoms in selected isomers of $CuSi_n$, Si_{n+1}, and $NaSi_6$ clusters ($n=4,6,8,10,12$).

Cluster		Cu/Na	Si(1)	Si(2)	Si(3)	Si(4)	Si(5)	Si(6)	Si(7)	Si(8)	Si(9)	Si(10)	Si(11)	Si(12)	Si(13)
$CuSi_4$	**4a**	0.47	−0.19	−0.19	0.04	−0.13									
	4b	0.48	−0.06	−0.36	0.10	−0.16									
	4c	0.51	−0.18	−0.18	−0.04	−0.11									
$CuSi_6$	**6a**	0.52	−0.25	−0.31	0.12	0.12	−0.10	−0.10							
	6a$^+$	0.65	−0.27	−0.41	0.02	0.52	0.40	0.09							
	6a$^-$	0.36	−0.33	−0.25	−0.16	−0.16	−0.23	−0.23							
	6b	0.64	−0.32	−0.32	−0.03	−0.03	0.03	0.03							
Si_7 (D_{5h})			−0.27	−0.27	0.11	0.11	0.11	0.11	0.11						
$NaSi_6$		0.90	−0.36	−0.36	−0.12	−0.12	0.03	0.03							
$CuSi_8$	**8a**	0.57	−0.20	−0.28	0.13	0.14	−0.16	−0.16	−0.02	-----	−0.03				
	8b	0.52	−0.13	−0.13	0.11	−0.11	−0.17	−0.35	0.13	0.13					
Si_9 (C_s)			−0.14	−0.14	0.15	0.17	−0.17	−0.20	0.07	0.07	0.19				
$CuSi_{10}$	**10a**	0.62	−0.33	−0.14	−0.13	−0.19	0.08	−0.03	0.01	0.00	−0.16	0.28			
	10b	0.49	−0.13	−0.13	−0.13	−0.12	−0.12	−0.12	−0.01	−0.01	−0.01	0.30			
	10c	0.57	−0.29	−0.29	−0.22	−0.02	−0.02	−0.15	-----	−0.03	−0.03	0.33	0.16		
Si_{11} (C_s-*II*)			−0.22	−0.22	−0.32	0.05	0.05	−0.19	0.12	0.04	0.04	0.42	0.23		
$CuSi_{12}$	**12a**	0.48	−0.08	0.02	−0.12	0.05	−0.12	0.02	0.05	−0.12	0.02	−0.08	0.02	−0.12	
	12d	0.60	−0.19	0.00	−0.19	0.00	−0.19	0.00	0.06	−0.07	0.08	−0.13	0.08	−0.07	
Si_{13} (C_{3v})			−0.05	−0.06	−0.05	−0.06	−0.05	−0.06	0.09	−0.04	0.09	−0.04	0.09	−0.04	0.16

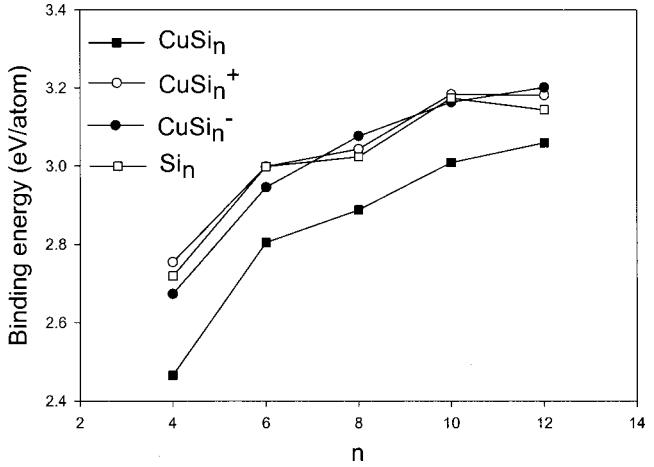

FIG. 3. Size dependence of the binding energy per atom (in eV/atom) for the most stable isomers of neutral and charged $CuSi_n$ as well as neutral Si_n clusters ($n=4-12$).

substitutional structures of Si_{11} (C_s-*II*) and Si_{11} (C_s-*I*), respectively, and **10a** and **10e** can be described either as two adsorption structures of Si_{10} (C_{3v}) or as substitutional structures of Si_{11}(C_1) and Si_{11}(C_s-*I*), respectively. Thus the most stable isomers of $CuSi_4$, $CuSi_6$ and $CuSi_{10}$ (**4a**, **6a**, and **10a**) all correspond to adsorption structures, in agreement with the magic feature of Si_4, Si_6, and Si_{10} clusters.

In addition, we have identified 12 other adsorption or substitutional isomers that are higher than **10a**–**10e** by 0.11–0.72 eV, of which one is an adsorption structure of Si_{10} (C_{3v}) with Cu capped over the 7Si-10Si bridge, five are substitutional structures of Si_{11}(C_s-*I*) with Cu at the 3Si (**10f** in Fig. 2), 4Si, 6Si, 7Si, and 9Si sites, three are substitutional structures of Si_{11} (C_s-*II*) with Cu at the 8Si, 10Si, and 11Si sites [the one with Cu occupying the 11Si site can also be counted as an adsorption structure of Si_{10} (C_{3v})], and three are substitutional structures of Si_{11} (C_{2v}) with Cu at the 3Si, 7Si, and 9Si sites, respectively. These isomers are not shown in Fig. 2, except **10f**, since this is the most stable isomer in the anionic charge state.

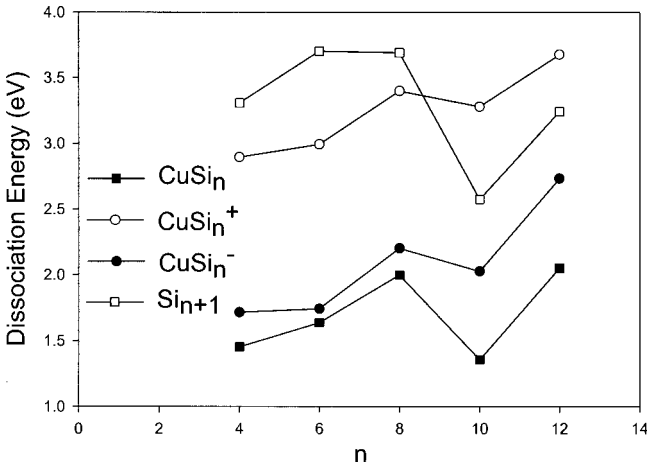

FIG. 4. Size dependence of the dissociation energy (in eV) for the most stable isomers of neutral and charged $CuSi_n$ clusters as well as neutral Si_{n+1} clusters ($n=4-12$).

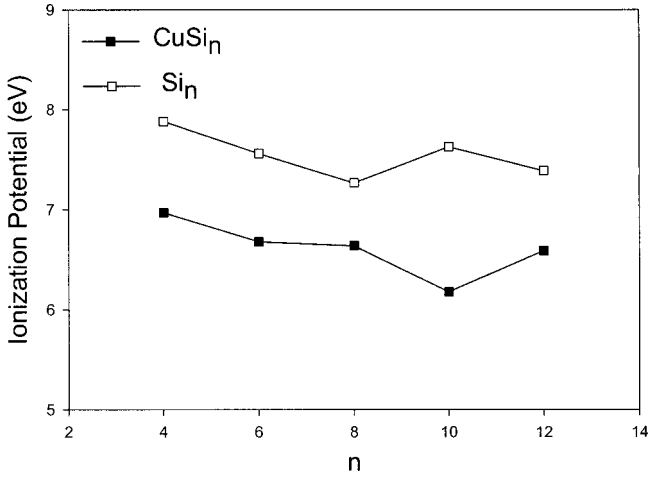

FIG. 5. Size dependence of the adiabatic ionization potential (in eV) for the most stable isomers of $CuSi_n$ and Si_n clusters ($n=4-12$).

The three center-site isomers **10g**, **10h**, and **10i** lie about 0.4 eV above **10a**–**10e** (Fig. 2 and Table III). In **10i**, Cu occupies the center of Si_{10} (C_{3v}). This structure is less stable by 0.42 eV than the corresponding adsorption structures (**10a**, **10b**, and **10e**), where Cu is adsorbed on various surface sites of Si_{10} (C_{3v}) (Table III).

By inserting Cu at the center of a tetracapped octahedron (T_d) of Si_{10} and relaxing the geometry, we have obtained two isomers. One is the center-site structure **10g** while the other is a substitutional structure of Si_{11} (C_{2v}) with Cu at the 3Si site, and the former is higher than the latter by 0.23 eV.

From the above comparison of **10g** and **10i** with corresponding adsorption and substitutional structures, we conclude that the center-site structures are still unfavorable for

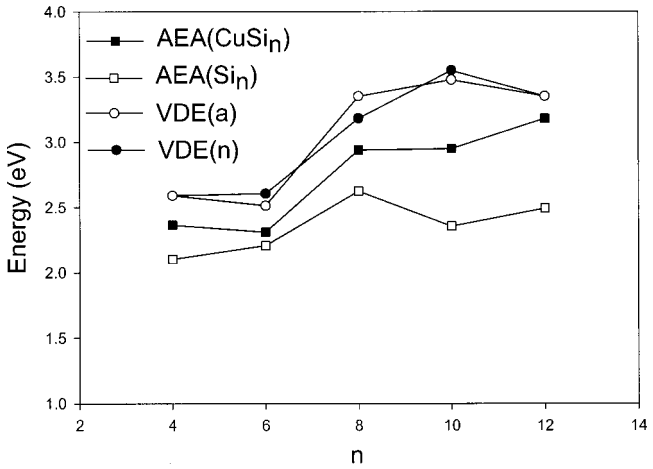

FIG. 6. Size dependence of the adiabatic electron affinity (AEA, in eV) for the most stable isomers of $CuSi_n$ and Si_n, and the vertical detachment energies (VDE, in eV) for $CuSi_n^-$ ($n=4-12$). For comparison, the VDEs calculated at the geometries of $CuSi_n^-$ corresponding to the most stable isomers of anionic $CuSi_n^-$ [open circle, VDE(a)] or of neutral $CuSi_n$ [solid circle, VDE(n)] species are both shown.

$CuSi_{10}$, but they become quite comparable in energy with the adsorption and substitutional structures.

We have also considered the insertion of Cu at the center of a bicapped tetragonal antiprism (D_{4d}) of Si_{10}. This highly symmetric cagelike D_{4d} structure was proposed by King[50] as a geometric model of $CuSi_{10}$, and was expected to show a high stability to account for the pronounced abundance of $CuSi_{10}$ as observed in Beck's mass spectrometric experiment.[18] Optimization at the B3LYP/6-311+$G(d)$ level, however, indicated that the D_{4d} structure of $CuSi_{10}$ is unstable and rearranges to the **10i** structure. From the above description, we know that there exist a number of low-lying isomers for $CuSi_{10}$ that exhibit a variety of structures and are very close in energy. For this reason, the high abundance of $CuSi_{10}$ observed in the mass spectrum[18] should not be ascribed to the geometric stability of a specific structure, but to the existence of a multitude of near-degenerate isomers.

We examined the influence of charge on the structures of all isomers of $CuSi_{10}$. The structures for the eight neutral isomers (**10b**–**10i**) shown in Fig. 2 are all essentially retained in both the cationic and the anionic forms, with $\mathbf{10e}^+$ and $\mathbf{10f}^-$ being the most stable among the respective charged species. The structure of neutral **10a** is maintained in the cationic form, but it transforms to a substitutional structure of Si_{11} (C_s-II) in anionic form (Fig. 2). As seen in Table III, the energy spacing between these isomers increases considerably when the clusters are charged, similar to the observations made for $CuSi_4$. Therefore, these isomers may be distinguishable more easily as cations or anions than as neutrals.

$CuSi_{12}$

12-atom clusters can form a number of highly symmetric cagelike structures with the following symmetries: icosahedron (I_h), octahedron (O_h), bicapped pentagonal antiprism (D_{5d}), hexacapped trigonal prism (D_{3h}), and hexagonal

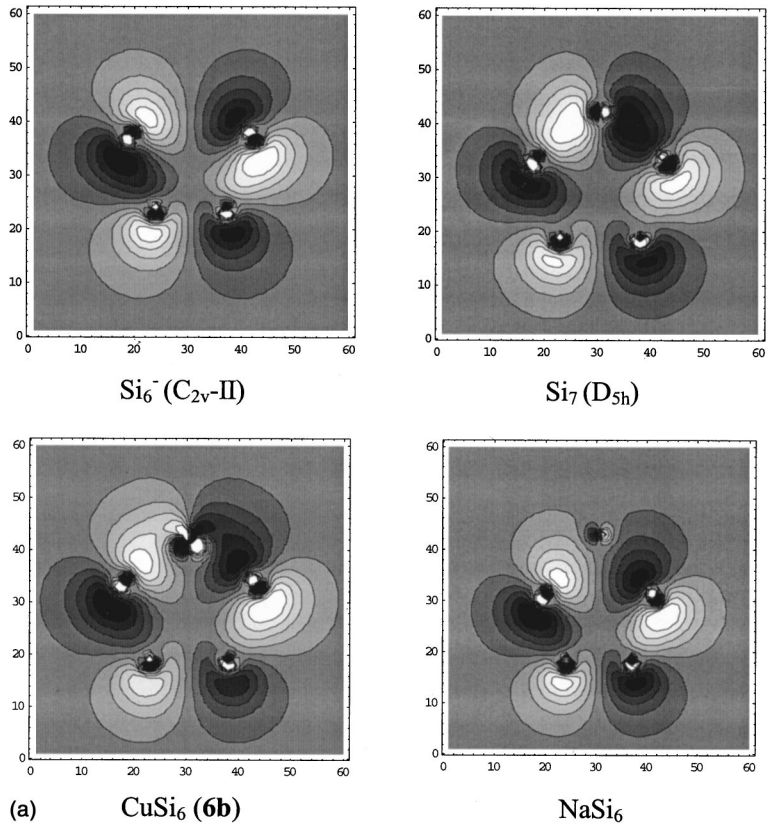

FIG. 7. (a) Contour maps (arbitrary units) for the HOMO's of Si_6^- ($C_{2v}-II$), Si_7(D_{5h}), $CuSi_6$ (**6b**), and $NaSi_6$ in the plane passing through the 3Si-6Si atoms. Cu and Na are on the top of the panel. (b) Contour maps (arbitrary units) for the HOMO's of Si_9 (C_s) and $CuSi_8$ (**8a**) in the plane passing through 5Si, 6Si, and 8Si (or Cu) atoms, with 8Si or Cu on the top of the panel, and the second HOMO of $CuSi_8$ (**8a**) in the plane passing through the 1Si, 2Si, 7Si, and Cu atoms, in which the 1Si and 2Si atoms are at the bottom, Cu is to the right, and 9Si is on the top of the panel but slightly off the plane. (c) Contour maps (arbitrary units) for the HOMO's of Si_{10}^- (C_{3v}) and $CuSi_{10}$ (**10a, 10b**, and **10c**) in the plane passing through the 3Si, 6Si, 10Si, and 7Si (or Cu for **10c**) atoms. (d) Contour maps (arbitrary units) for the HOMO's of Si_{13} (C_{3v}) and $CuSi_{12}$ (**12d**) in plane *A* passing through the 1Si, 4Si, 7Si, and 10Si atoms, and the second HOMO of $CuSi_{12}$ (**12a**) in plane *A*, and in plane *B* passing through the 2Si, 3Si, 5Si, and 6Si atoms. (e) The diagonal bond between the 1Si and 8Si atoms: contour maps (arbitrary units) for the HOMO's of Si_{13} (C_{3v}), $CuSi_{12}$ (**12a** and **12d**) in the plane passing through the 1Si-2Si-7Si-8Si rhombus with 7Si and 8Si at the bottom of the panel. Note that only the 1Si, 7Si, and 8Si atoms are exactly in the plane while the 2Si atom is slightly off it for Si_{13} (C_{3v}) and **12d** because of the distortion of the rhombus. For **12a**, the distortion of the rhombus is considerably reduced as compared with Si_{13} (C_{3v}), and the four atoms can be seen in the plane.

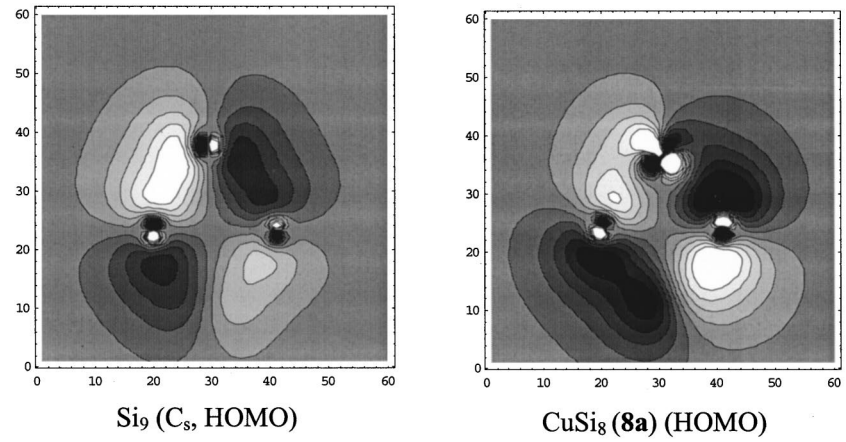

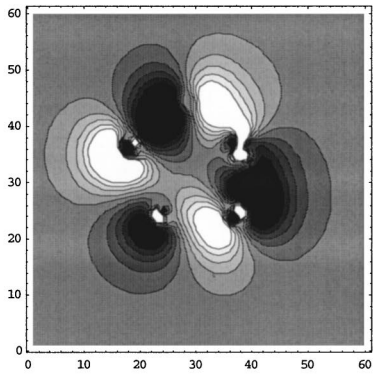

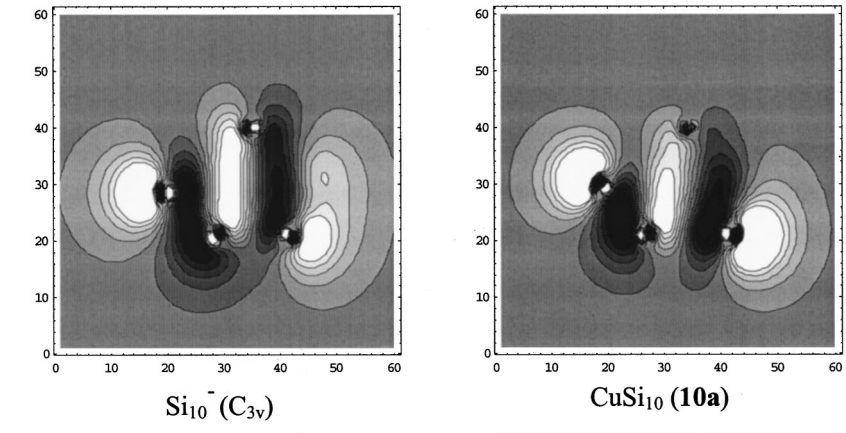

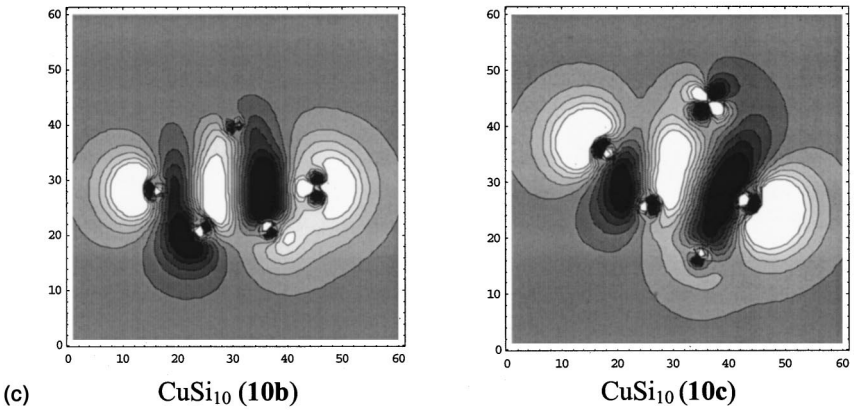

FIG. 7. (*Continued.*)

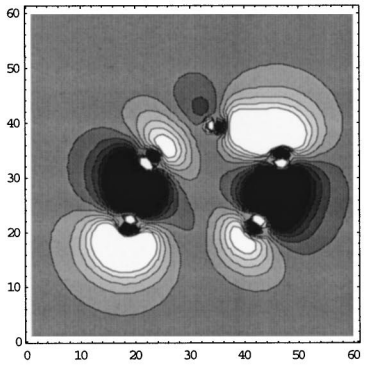

Si_{13} (C_{3v})

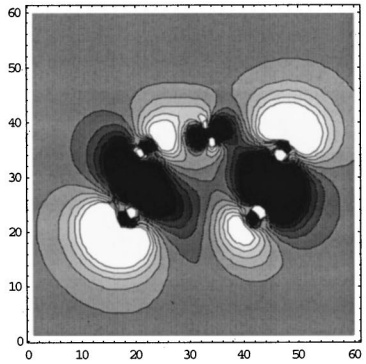

$CuSi_{12}$ (**12d**)

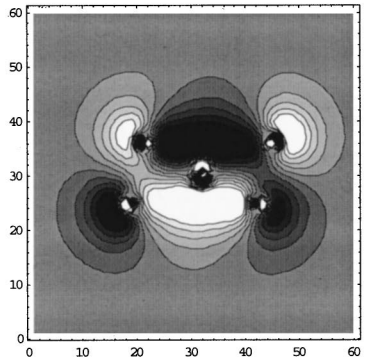

(d) $CuSi_{12}$ (**12a**) (2nd HOMO, **A**)

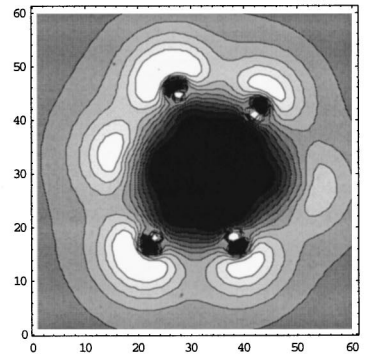

$CuSi_{12}$ (**12a**) (2nd HOMO, **B**)

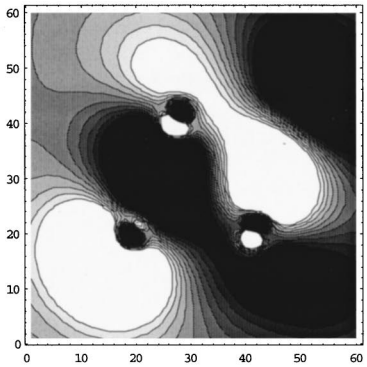

Si_{13} (C_{3v})

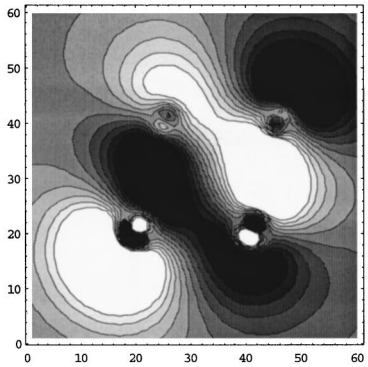

$CuSi_{12}$ (**12a**)

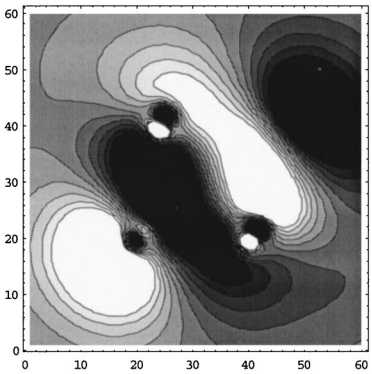

(e) $CuSi_{12}$ (**12d**)

FIG. 7. (*Continued.*)

prism (D_{6h}). The Si_{12} cluster provides a suitable test case for the exploration of the question: Can Cu stabilize cagelike Si_n structures?

Based on the cagelike frameworks indicated above as well as the ground-state and low-lying structures of Si_{12} and Si_{13} (Fig. 1), we performed an extensive search for stable isomers of $CuSi_{12}$. Altogether, we identified 12 isomers for $CuSi_{12}$ which can be classified into two types: nine substitutional structures (with one also belonging to the adsorption type) and three center-site structures; five selected isomers of these are plotted in Fig. 2.

In contrast to $CuSi_4$ through $CuSi_{10}$, where the most stable isomer is derivable from the ground-state structure of Si_n^- (**4a**, **6a**, **10a**) or Si_{n+1} (**8a**) with Cu at an adsorption or a substitutional site, the lowest isomer of $CuSi_{12}$ adopts the shape of a cagelike hexagonal double-chair (**12a**) with Cu at the center of the cage (Fig. 2). This geometry does not correspond to the ground-state structures of Si_{12} (C_s-*I*) or Si_{13} (C_{2v}), but is related to a higher-lying isomer of Si_{13} (C_{3v}). Similar results was reported for metallofullerenes, namely, a discrepancy between the cage structure of some endohedral metallofullerenes and the structure of the most stable isomer of pure fullerenes.[51]

It is worth noting that **12a** is quite similar to the regular hexagonal prism recently proposed in Ref. 23 as the ground-state structure of WSi_{12}. We have found that, if Cu is replaced by W in our center-site isomer **12a**, relaxation will lead to the regular hexagonal prism structure of WSi_{12}.[27,52] However, charge transfer between the metal and the Si_{12} framework in these two systems are found to proceed in opposite directions and their bonding characters are found different.[52]

Isomer **12a** can be obtained from several different starting geometries. One arrives at this unit by inserting a Cu atom at the center of the Si_{12} (D_{3h} or D_{6h}) cage, by adsorbing a Cu atom on a face of the Si_{12} (O_h) cage, or by substituting a Cu atom for the 13Si atom of Si_{13} (C_{3v}) and moving it to the center of the double-chair framework.

The **12a** structure has some similarity to bulk Si, as have **6c** and **8d**. Note that the chairlike structure appears as the least stable isomer both for $CuSi_6$ and for $CuSi_8$, but it turns out to be the most stable for $CuSi_{12}$, implying that some bulklike behavior might emerge in $CuSi_{12}$. As will be shown in Sec. III D below, the bonding nature in **12a** also reveals interesting features. Of course, the **12a** structure is still quite different from the bulk, since the binding energy of **12a** (3.06 eV/atom) is much smaller than that of bulk Si (4.64 eV/atom),[5] and the relative positions of the double chairs in **12a** and in bulk Si are different.

In addition to **12a**, we have found two other endohedral geometries of $CuSi_{12}$, in which the Cu atom is at the center of Si_{12} (C_s-*II*) (**12e** in Fig. 2) and Si_{12} (D_{5d} or I_h) (not shown in Fig. 2). These isomers are, however, much higher in energy than **12a**, by 0.86 and 1.74 eV, respectively.

The remaining nine isomers all belong to the substitutional group, of which four are substitutional structures of Si_{13} (C_{2v}) with Cu at the 7Si site (**12b** in Fig. 2) and the 8Si, 10Si and 13Si (**12c** in Fig. 2) sites; four are substitutional structures of Si_{13} (C_s) with Cu at the 2Si, 4Si, 8Si, and 13Si sites; and one is a substitutional structure of Si_{13} (C_{3v}) with Cu at the 13Si site (**12d** in Fig. 2). These isomers are higher than the most stable isomer **12a** by 0.28–1.27 eV. The substitutional isomer **12c** can also be classified as an adsorption structure of Si_{12} (C_s-*II*) and it is the only adsorption structure we have identified for $CuSi_{12}$.

Isomers **12c** and **12e** are both derived from the ground state of Si_{12} (C_s-*I*) with Cu at an adsorption site or at the center, respectively. In both isomers, the Si_{12} framework transforms to that of Si_{12} (C_s-*II*), which is the ground state of Si_{12}^-, and these two isomers are higher than the most stable isomer **12a** by 0.34 and 0.86 eV respectively, indicating that the growth pattern of $CuSi_n$ based on the ground-state structures of Si_n or Si_{n+1}, as observed in $CuSi_4$ through $CuSi_{10}$, becomes unfavorable at $n=12$; thus the systematics of the $CuSi_n$ size evolution is expected to change as $n \geqslant 12$.

It is interesting to compare the relative stability of the center-site structure **12a** and corresponding substitutional structure **12d**, both of which have a double-chair framework of Si_{12}. From Table III, one finds that **12a** is more stable than **12d** by 0.35 eV, showing a clear preference of the center-site structure over the substitutional structure for $CuSi_{12}$.

From the above description and Table III, one can also find that **12a** is clearly lower than all other isomers we have identified for $CuSi_{12}$ by at least 0.28 eV. This finding contrasts with the cases of $CuSi_n$ ($n=4,6,8,10$) where several competitive isomers exist as candidates for the ground state of the cluster. Whether the cluster is positively or negatively charged, the structures for isomers **12a–12e** shown in Fig. 2 are all retained, and $\mathbf{12b}^+$ becomes the most stable isomer in the cationic charge state which is lower than $\mathbf{12a}^+$ by 0.24 eV.

C. Energetic properties

Based on the above geometric results, we have calculated the binding energy per atom (E_b) and the dissociation energy (D_e) for all isomers shown in Fig. 2 in the neutral and charged forms (Table III). The overall stability of $CuSi_n$ can be characterized by the binding energy per atom with respect to isolated atoms:

$$E_b(\mathrm{CuSi}_n)=[E(\mathrm{Cu})+nE(\mathrm{Si})-E(\mathrm{CuSi}_n)]/(n+1),$$

$$E_b(\mathrm{CuSi}_n^+)=[E(\mathrm{Cu}^+)+nE(\mathrm{Si})-E(\mathrm{CuSi}_n)]/(n+1),$$

$$E_b(\mathrm{CuSi}_n^-)=[E(\mathrm{Cu})+(n-1)E(\mathrm{Si})+E(\mathrm{Si}^-)-E(\mathrm{CuSi}_n)]/(n+1),$$

while the interaction of Cu with the Si_n framework can be characterized by the dissociation energy with respect to $Cu+Si_n$:

$$D_e(\mathrm{CuSi}_n)=E(\mathrm{Cu})+E(\mathrm{Si}_n)-E(\mathrm{CuSi}_n),$$

$$D_e(\mathrm{CuSi}_n^+)=E(\mathrm{Cu}^+)+E(\mathrm{Si}_n)-E(\mathrm{CuSi}_n),$$

$$D_e(\mathrm{CuSi}_n^-)=E(\mathrm{Cu}+E(\mathrm{Si}_n^-)-E(\mathrm{CuSi}_n).$$

Figure 3 shows the size dependence of the binding energy per atom for the most stable isomers of $CuSi_n$ in the neutral (**4a**, **6a**, **8a**, **10a**, and **12a**), cationic (**4b**$^+$, **6a**$^+$, **8a**$^+$, **10e**$^+$ and **12b**$^+$), and anionic (**4a**$^-$, **6b**$^-$, **8a**$^-$, **10f**$^-$, and **12a**$^-$) charge states. For comparison, the size dependence of the binding energy per atom for neutral Si_n calculated at the B3LYP/6-311+$G(d)$ level is also shown.

First, we compare the size dependence of the binding energy for neutral $CuSi_n$ and Si_n clusters. Both curves reveal the same size dependence with enhanced stability at $n=6$ and 10, and possibly also at $n=4$. This result indicates that the stability of $CuSi_n$ can be related to the stability of pure Si_n.

The enhanced stability of $CuSi_{10}$ may be regarded as a factor that contributes to the pronounced abundance of $CuSi_{10}$ as observed in Beck's mass spectrometric experiment.[18] This is in addition to the contribution of the high multiplicity of nearly isoenergetic low-lying isomers of this species.

Furthermore, our results indicate that $CuSi_4$ and $CuSi_6$ may also have considerable stability, a finding that is in agreement with the more recent experiment of Scherer *et al.*[19] which demonstrated that copper silicide clusters with less than six Si atoms can be formed in high abundance.

Next we compare the size dependence of the binding energies for $CuSi_n$ in the neutral and charged forms. The curve for $CuSi_n^+$ shows a size dependence similar to that for neutral $CuSi_n$, and the enhanced stability of $CuSi_6$ and $CuSi_{10}$ is even more obvious in the cationic form. The curve for $CuSi_n^-$ is, however, rather smooth, so that nearly no magic feature is observable at $CuSi_6^-$ and $CuSi_{10}^-$. It follows that different patterns for the cationic and the anionic species can arise in mass spectroscopy and other experiments. It should be noted that the mass spectrometric measurements of Beck[18] and of Scherer *et al.*[19] were both performed for cationic species. The present analysis suggests that similar results should be expected for the neutral species.

Figure 4 shows the size dependence of the dissociation energy for the most stable isomers of $CuSi_n$ in all charge states. Also plotted in Fig. 4 is the size dependence of the dissociation energy for neutral Si_{n+1} with respect to Si $+Si_n$ determined at the B3LYP/6-311+$G(d)$ level. One finds that the dissociation energy for $CuSi_n$ shows a similar size dependence in all charge forms with minima at $n=6$ and 10. This means that Cu stabilizes the Si_n framework to a lesser extent in $CuSi_6$ and $CuSi_{10}$ than in other $CuSi_n$ clusters. This finding is consistent with the exceptional stability of Si_6 and Si_{10}, and therefore less stabilization effect can be anticipated by addition of a Cu atom to these systems than to the other Si_n units studied here.

On the other hand, the curve for the dissociation energy of neutral $CuSi_n$ lies consistently and substantially lower than that of neutral Si_{n+1}, indicating that the Cu-Si interaction is much weaker than the Si-Si interaction, in agreement with the conclusion drawn from analysis of CuSi and Si_2 dimers (Table I). Because of the much weaker Cu-Si interaction, the Si-Si bonding is dominant in the $CuSi_n$ clusters and this explains why the stability and even the framework of $CuSi_n$ can be related to that of Si_n.

The size dependence of the dissociation energies for $CuSi_n$ and Si_{n+1} shows a striking difference around $n=6$. This difference comes from the enhanced stabilization effect on the Si_6 framework of the extra Si atom, i.e., the 7Si atom of Si_7 (D_{5h}), as compared to the Cu atom of $CuSi_6$. The exceptional stability of Si_7 (D_{5h}) is ascribed to its special geometric arrangement, i.e., a highly symmetric close-packed-pentagonal bipyramid (Fig. 1), and the resulting strong bonding interaction. The extra 7Si atom of Si_7 (D_{5h}) acts as one of the five equivalent equatorial atoms among which a strong bond is formed in the HOMO (highest occupied molecular orbital), as shown in Sec. III (D) below. This special symmetric arrangement is destroyed in the most stable isomer of $CuSi_6$ in all charge forms (**6a**,**6a**$^+$,**6b**$^-$) and the Cu atom has a much weaker bonding interaction with the Si atoms. Therefore, the enhanced stabilization effect of the extra 7Si atom on the Si_6 framework disappears when it is replaced by Cu.

In addition to the binding and dissociation energies, we have also calculated the adiabatic ionization potential (AIP) and the adiabatic electron affinity (AEA) for all neutral $CuSi_n$ species presented in Fig. 2 as well as the vertical detachment energy (VDE) for corresponding anionic $CuSi_n^-$ species, which are defined as the difference of total energies in the following ways:

AIP: E(optimized cation)-E(optimized neutral),
AEA: E(optimized neutral)-E(optimized anion),
VDE: E(neutral at optimized anion geometry)-
E(optimized anion).

From the definition, the VDE will be larger than the AEA, and their difference reflects the geometric relaxation of the cluster from the anion to the neutral. The calculated results are tabulated in Table IV and shown in Figs. 5 and 6. We expect that these data will stimulate further experimental studies of $CuSi_n$ clusters.

From Table IV, we see that the values of the AIP, AEA, and VDE for different isomers of $CuSi_n$ are quite close and they do not change much with cluster size. The former conclusion implies that different isomers of a cluster may hardly be distinguishable by measuring these quantities. For most isomers, the VDE is larger than corresponding AEA by 0.2–0.3 eV. However, there are several cases (**4c**, **10a**, **10g**) where the VDE exceeds the corresponding AEA by as much as 0.5–0.6 eV, indicating that a considerable rearrangement in the cluster geometry is associated with the removal of the extra electron from the anion.

Figures 5 and 6 show, respectively, the size dependence of the AIP and AEA for the most stable isomers of $CuSi_n$ and Si_n. The curve for the AEA of $CuSi_n$ (Fig. 6) reveals a similar size dependence to Si_n and, for all cluster sizes, the AEA for $CuSi_n$ is larger than the values for the Cu and the Si atoms (Table I) and for the corresponding Si_n cluster (Fig. 6). In contrast, the AIPs for $CuSi_n$ and Si_n (Fig. 5) show different size dependencies and, for all cluster sizes, the $CuSi_n$ units have smaller AIP values than those found for the Cu and Si atoms (Table I) and for the corresponding Si_n cluster (Fig. 5). If we compare the curve for the AIP of $CuSi_n$ in Fig. 5 with the curve for the dissociation energy of $CuSi_n$ in Fig. 4, we find local minima at $n=6$ and, more remarkably, at

$n=10$ in both curves, implying that the ionization potential of the $CuSi_n$ cluster is related to the Cu-Si interaction.

Finally, the size dependence for the VDE of anionic $CuSi_n^-$ species is also shown in Fig. 6. For comparison, the VDEs calculated at the geometries of the $CuSi_n^-$ species corresponding, respectively, to the most stable isomers of anionic $CuSi_n^-$ clusters [**4a**$^-$, **6b**$^-$, **8a**$^-$, **10f**$^-$ and **12a**$^-$, denoted by open circles and VDE(a) in Fig. 6] and to the most stable isomers of neutral $CuSi_n$ clusters [**4a**$^-$, **6a**$^-$, **8a**$^-$, **10a**$^-$ and **12a**$^-$, denoted by the solid circle and VDE(n) in Fig. 6] are both shown. The size dependencies for VDE(a) and VDE(n) are quite similar, and they are different from the size dependence of the AEA for $CuSi_n$ only at $n=10$, indicating that the rearrangement is larger in $CuSi_{10}$ than in other cluster sizes when the cluster is negatively charged. Indeed, the structures for the most stable isomers of $CuSi_n$ are largely retained at $n=4$, 6, 8, and 12 (**4a**, **6a**, **8a**, and **12a**) when the clusters are negatively charged, with a small difference between the VDE and AEA of 0.18–0.30 eV, while the structure for the most stable isomer of $CuSi_{10}$ (**10a**) rearranges to another structure in the anionic form (Fig. 2), where the VDE and AEA differ by 0.60 eV (Table IV).

D. Bonding properties

In this subsection, the Cu-Si bonding properties in the representative isomers of neutral $CuSi_n$ clusters are analyzed. At the B3LYP/GEN level, we found that the *d* shell of Cu in all isomers of $CuSi_4$ and $CuSi_6$ clusters remains nearly closed.[28] This conclusion is confirmed by the present calculation at the B3LYP/6-311+$G(d)$ level, as can be seen from Table VI, where the natural electronic configurations for the Cu atom in representative isomers of $CuSi_n$ ($n=4,6,8,10,12$) are tabulated. Therefore, the *d* shell of Cu is expected to play only a small role in Cu-Si bonding. Since the bonding in $CuSi_4$ has been analyzed in detail at the B3LYP/GEN level[28] and the results are similar at the B3LYP/6-311+$G(d)$ level, no further description of this cluster will be given here and we start with $CuSi_6$.

$CuSi_6$

Among the three isomers identified for $CuSi_6$, **6a** and **6b** are two competitive candidates for the ground state and represent adsorption and substitutional structures, respectively. The geometry of Si_6 framework is close to Si_6^- (C_{2v}-*II*) in both isomers. Natural population analysis (NPA) indicates that the electron transfers in **6a** and **6b** are, respectively, 0.52*e* and 0.64*e* from Cu to the Si_6 framework (Table V). Therefore, the structural and charge-transfer features both suggest that the electronic structures of **6a** and **6b** would correspond to that of Si_6^- (C_{2v}-*II*). For the substitutional isomer **6b**, it is desirable to examine how the Cu atom will modify the electronic structure of the substituted Si atom in Si_7 (D_{5h}).

Examining the molecular orbitals, we find that the HOMOs of **6a**, **6b**, and Si_7 (D_{5h}) all clearly correspond to the lowest unoccupied molecular orbital of Si_6 (C_{2v}-*II*) or the HOMO of Si_6^- (C_{2v}-*II*). This is consistent with electron transfer proceeding from Cu to Si_6 as suggested by NPA. A comparison of the HOMOs for Si_6^- (C_{2v}-*II*), Si_7 (D_{5h}) and **6b** in the plane passing through the equatorial plane (3Si to 6Si) is shown in Fig. 7(a).

The HOMO of Si_6^- (C_{2v}-*II*) consists almost completely of orbitals from the equatorial atoms, i.e., a dominant contribution (57.3%) from the *p* orbitals of 3Si and 4Si atoms and a large contribution (30.5%) from the *s* and *p* orbitals of 5Si and 6Si atoms. This leads to strong bonds in the 3Si-5Si and 4Si-6Si bridges, but antibonding connections in the 3Si-4Si and 5Si-6Si pairs [Fig. 7(a)]. The contribution of the 1Si and 2Si atoms to the HOMO of Si_6^- (C_{2v}-*II*) is small (4% *p* in the 3Si-4Si direction), resulting in very weak bonding between them.

The bonding character among the 1Si to 6Si atoms of Si_6^- (C_{2v}-*II*) is essentially retained in the HOMOs of Si_7 (D_{5h}), **6a** and **6b** [Fig. 7(a)]. For Si_7 (D_{5h}), the top equatorial atom 7Si has a large *p* character (25.1% *p*) in the HOMO and forms strong bonds with the neighboring equatorial atoms 3Si and 4Si [Fig. 7(a)]. For the substitutional isomer **6b**, the Cu atom has 13.0% *p* and 3.2% *d* characters in the HOMO. Therefore, Cu behaves quite similar to the replaced Si atom, reproducing a relatively strong bond with the neighboring equatorial atoms 3Si and 4Si [Fig. 7(a)]. The Cu-Si bond, however, is still much weaker than the Si-Si bond since the contribution of Cu to the HOMO of **6b** is only half that of 7Si to the HOMO of Si_7 (D_{5h}). Concerning the HOMO of the adsorption isomer **6a**, it has only 1.1% *d* and 0.9% *p* characters on Cu, and shows a striking similarity to the HOMO of Si_6^- (C_{2v}-*II*) in the equatorial plane. The HOMO of **6a** is hence not shown in Fig. 7(a).

NPA indicates that, for Si_7 (D_{5h}), the positive charge resides on the five equatorial atoms (3Si to 7Si, each 0.11*e*) while negative charge is found on the two apex atoms (1Si and 2Si, each $-0.27e$) (Table V). The charge on Cu of the substitutional isomer **6b** is similar to the equatorial but opposite to the apex Si atoms of Si_7 (D_{5h}). This explains why substitution of Cu for the equatorial atoms of Si_7 (D_{5h}) retains stability, but substitution of Cu for the apex atoms leads to a large reconstruction. Since the charge on Cu is transferred almost entirely to the two apex atoms 1Si and 2Si in **6b**, the Cu atom interacts with the adjacent equatorial atoms 3Si and 4Si through covalent bonding while it interacts with the apex atoms 1Si and 2Si through an ionic interaction. In the adsorption isomer **6a**, the equatorial atoms 5Si and 6Si that are close to Cu also acquire negative charges, in addition to the adjacent apex atom 2Si. Therefore, the Cu atom in **6a** is bound to the Si_6 framework mainly through an ionic interaction.

It is interesting to compare the substitutional isomer **6b** with $NaSi_6$ which has a similar structure.[22] This cluster was determined by Kishi *et al.*[22] as the ground state of $NaSi_6$ and reoptimized at the B3LYP/6-311+$G(d)$ level. NPA indicates that there is an electron transfer of as large as 0.90*e* from Na to its neighboring atoms (1Si to 4Si) in the substitutional $NaSi_6$ structure (Table V). The Na atom in $NaSi_6$ donates its valence electron almost completely to the Si_6 framework and behaves like a Na^+ ion (Tables V and VI),

leading to a nearly purely ionic interaction between Na and the Si_6 framework. Indeed, the HOMO of $NaSi_6$, which is shown in Fig. 7(a) has only 4.1% *p* character on Na. Note that the $3p$ orbital of Na has one radial node and the delocalized outer part is too diffuse and weak to be visible in the figure. This bonding mechanism is similar to the predominantly ionic Cu-Si interaction in the adsorption isomer **6a** but unlike the mixed covalent and ionic Cu-Si interaction prevailing in the substitutional isomer **6b**.

$CuSi_8$

The two most stable isomers **8a** and **8b** are also nearly isoenergetic and represent substitutional and adsorption structures, respectively. Similar to $CuSi_6$, the electronic structure of **8a** and **8b** can be understood by reference to Si_8^- (C_{2v}) and Si_9 (C_s).

The structure of Si_9 (C_s) can be regarded as a Si_8 (C_{2v}) framework capped atop with a 9Si atom (Fig. 1). The HOMO of Si_9 (C_s) has large *p* coefficients on the atoms from 1Si through 8Si but only 1.9% *p* character on 9Si. This leads to a delocalized bonding among the atoms in the upper (1Si to 4Si) and lower (5Si to 8Si) rhombi while the interaction between these two rhombi is weakly antibonding. The components of the HOMOs of the substitutional isomer **8a** and of Si_9 (C_s) on corresponding Si atoms are very similar. The contribution of Cu to the HOMO of **8a** consists of 8.3% *p* and 3.4% *d* characters, while the contribution of the replaced 8Si atom to the HOMO of Si_9 (C_s) amounts to 13.2% *p* character. A comparison of the HOMOs of Si_9 (C_s) and **8a** in the plane passing through 8Si (or Cu) and two neighboring atoms 5Si and 6Si can be found in Fig. 7(b). Just like the substitutional structure **6b**, the Cu atom of **8a** exhibits a similar bonding pattern to the replaced 8Si atom of Si_9 (C_s).

We have examined the second HOMO of **8a** and found an interesting connection to Si_7 (D_{5h}). The contour map for the second HOMO of the substitutional structure **8a** in the plane passing through Cu, 1Si, 2Si, and 7Si atoms is shown in Fig. 7(b), in which the 1Si and 2Si atoms are at the bottom, Cu is to the right, and 9Si is on the top of the panel but slightly off the plane. If we compare this bonding pattern with the HOMO of **6b** in the equatorial plane [Fig. 7(a)], a striking similarity emerges. This bonding similarity roots in the structural analogy of the two cluster species. As seen in Fig. 1, the structure of Si_9 (C_s) can be viewed as a distorted framework of Si_7 (D_{5h}) bicapped with 3Si and 4Si atoms. For a quantitative demonstration of this structural relationship, one may compare the geometric data for the pentagonal ring (1Si, 2Si, and 7Si to 9Si) of Si_9 (C_s) with the pentagonal equator of Si_7 (D_{5h}). The 9Si-7Si, 7Si-1Si, and 1Si-2Si bond lengths for Si_9 (C_s) are 2.49, 2.54, and 2.62 Å, respectively, while the 8Si-9Si-7Si, 9Si-7Si-1Si, and 7Si-1Si-2Si bond angles are, respectively, 107.46°, 108.29°, and 105.89°. These values are close to the corresponding bond lengths of 2.51 Å and bond angles of 108.0° for the pentagonal equator of Si_7 (D_{5h}). The Cu atom of **8a** is located at one of the equatorial sites, leading to the similarity of the second HOMO for **8a** with the HOMO for **6a**. The change in the order of molecular orbitals reflects the influence of the capped 3Si and 4Si atoms.

For the adsorption isomer **8b**, the contribution of Cu to the HOMO is very small, while the bonding nature among Si atoms in the HOMO is quite similar to that among corresponding Si atoms in the HOMO of Si_9 (C_s). Therefore, the Cu-Si bonding is quite weak in **8b**. On the other hand, Cu has a positive charge of $0.52e$, whereas the natural charges on the adjacent 4Si and 6Si atoms are both negative, being $-0.11e$ and $-0.35e$, respectively (Table V). Therefore, the Cu atom is bound to the Si_8 framework of **8b** mainly through an ionic interaction, similar to the case of the adsorption structure **6a**.

$CuSi_{10}$

$CuSi_{10}$ has five nearly isoenergetic isomers (**10a**–**10e**) as competitive candidates for its ground state, one of which is a typical adsorption structure (**10b**), two are typical substitutional structures (**10c** and **10d**), and two can be subsumed under either category (**10a** and **10e**). We choose to analyze the bonding in the representative **10a**, **10b**, and **10c** isomers.

The electronic properties of **10a**, **10b**, and **10c** can all be related to Si_{10}^- (C_{3v}). The structure of Si_{10}^- (C_{3v}) is a capped TTP and consists of four layers along the trigonal axis (3Si-6Si direction) (Fig. 1). Its HOMO has large *p* components on all atoms orienting along the trigonal axis. In addition, all atoms except the 4Si-5Si-6Si layer also contribute large *s* components to the HOMO. As a result, strong delocalized bonds are formed among the three atoms of each layer and between adjacent layers along the trigonal axis, making this geometry exceptionally stable. The contour map of this HOMO in a typical plane passing through the trigonal axis and the 3Si, 6Si, 7Si, and 10Si atoms is shown in Fig. 7(c). One finds that the HOMO exhibits alternative positive and negative patterns along the trigonal axis.

The HOMOs of **10a**, **10b**, and **10c** all correspond to the HOMO of Si_{10}^- (C_{3v}), showing similar alternating positive and negative patterns in the 3Si-6Si direction [Fig. 7(c)]. For the adsorption isomer **10b**, the HOMO has large *s*, considerable *p* as well as small *d* components on Cu and these components well match the positive lobe of the *p* orbitals of the atoms on the 4Si-5Si-6Si face of **10b**. Therefore, the Cu atom of **10b** is bound strongly to the 4Si-5Si-6Si face of the Si_{10} framework.

For the substitutional isomer **10c**, the Cu atom has considerable *s* and *p*, and small *d* components in the HOMO. Therefore, Cu interacts quite strongly with neighboring Si atoms in **10c**.

Similar to the adsorption isomer **10b**, the Si_{10} (C_{3v}) framework is largely retained and the Cu atom is capped to a face of three atoms, 1Si-4Si-9Si, in **10a** (Fig. 2). The contribution of Cu to the HOMO of **10a** consists of considerable *s* and small *p* characters, which is also similar to the case of **10b**. However, since the three atoms of the capping face (1Si, 4Si, and 9Si) in **10a** are situated in different layers of the Si_{10} (C_{3v}) framework and they have dominant *p* characters in the HOMO that are different in phase at the Cu site, the Cu *s* orbital cannot overlap effectively with the *p* orbitals of the 1Si, 4Si, and 9Si atoms, leading to a weak interaction between Cu and the 1Si-4Si-9Si face.

NPA indicates that Cu has positive charges of $0.62e$, $0.49e$, and $0.57e$ while the neighboring Si atoms carry negative charges of $-0.68e$, $-0.36e$, and $-0.62e$ in **10a**, **10b**, and **10c**, respectively (Table V). It seems that the ionic interaction has a more important role in **10a** than in **10b** and **10c**. The bonding feature revealed in **10a** is similar to those found in the adsorption structures of **6a** and **8b** and the isomer **10a** may, therefore, be better classified as an adsorption structure.

$CuSi_{12}$

In contrast to smaller $CuSi_n$ ($n=4,6,8,10$) clusters, the lowest isomer of $CuSi_{12}$ is a cagelike double-chair structure (**12a**) with Cu at the center site. We focus on the analysis of bonding features of the center-site isomer **12a** and corresponding substitutional isomer **12d**.

The electronic properties of **12a** and **12d** can both be related to Si_{13} (C_{3v}). The structure of Si_{13} (C_{3v}) consists of hexagonal double chairs capped atop with a Si atom. Six distorted rhombi can be discerned within double chair arrangement (Fig. 1). The HOMO of Si_{13} (C_{3v}), which is composed of small *p* components on the top 13Si atom, but large *p* and *s* coefficients on the atoms of the double chairs, is doubly degenerate. Strong delocalized bonds are formed among the atoms of each chair and between adjacent atoms of the two chairs, while the top 13Si atom is weakly bound to the 2Si, 4Si, and 6Si atoms of the upper chair, as shown in Fig. 7(d).

In addition, a noticeable diagonal interaction is found among all atoms on the short diagonals of the six distorted rhombi of the double chairs, i.e., among the 1Si-8Si-3Si-10Si-5Si-12Si-1Si atoms, of Si_{13} (C_{3v}), forming a chair-like cyclic diagonal bond. For example, Figure 7(e) displays the HOMO of Si_{13} (C_{3v}) in the plane passing through the 1Si-2Si-7Si-8Si rhombus. Since the rhombus is distorted, only the 1Si, 7Si, and 8Si atoms are exactly on the plane while the 2Si atom is slightly off. One sees that a diagonal bond is formed through the 1Si-8Si interaction. Because of the existence of the diagonal bond, the 1Si atom is pulled down by interaction with 8Si and 12Si atoms while 8Si moves up by interaction with 1Si and 3Si atoms, leading to a puckered structure of the double chairs (Fig. 1).

The HOMOs of the center-site isomer **12a** and the substitutional isomer **12d** are both derivable from the HOMO of Si_{13} (C_{3v}). The delocalized bond among the atoms of the double chairs and the diagonal bond still exist in **12a** and **12d** [Fig. 7(e)], but the diagonal bonding and hence the puckering of the double chairs diminish as one goes from Si_{13} (C_{3v}) to **12b** to **12a**. This can be seen from a comparison of the average lengths of the short and long diagonals ($\overline{R}_1$,$\overline{R}_2$) and corresponding average opening angles ($\overline{A}_1$,$\overline{A}_2$) of the rhombi in the double chairs of these clusters. For clarity, we take the 1Si-2Si-7Si-8Si rhombus as an example to explain the meanings of these quantities. R_1 and R_2 correspond to the lengths of 1Si-8Si and 2Si-7Si while A_1 and A_2 are defined as the average of 2Si-1Si-7Si and 2Si-8Si-7Si angles or the average of 1Si-2Si-8Si and 1Si-7Si-8Si angles, respectively. $\overline{R}_1$, $\overline{R}_2$, $\overline{A}_1$, and $\overline{A}_2$ are the averages of R_1, R_2, A_1 and A_2 over all rhombi of the double chairs. The R_1 and R_2 values for Si_{13} (C_{3v}) are 2.68 and 3.95 Å, while the corresponding $\overline{R}_1$ and $\overline{R}_2$ values are 2.83 and 3.81 Å for **12d**, and 3.01 and 3.72 Å for **12a**. The $\overline{A}_1$ and $\overline{A}_2$ values in Si_{13} (C_{3v}) are 109.33° and 67.21°. They change to 103.91° and 71.64° in **12d**, and 101.05° and 77.36° in **12a**. The Cu atom tends to reduce the distortion of the double-chair framework and regularize it toward the perfect hexagonal prism of D_{6h} symmetry. As will be rationalized below, this effect of regularization, as compared with Si_{13} (C_{3v}), can be ascribed to the tendency of Cu to bond with more Si atoms than the 13Si atom and, as shown in Table V, the interaction between Cu and Si_{12} is characterized by considerable charge transfer and hence by a substantial ionic bonding component. The trend of the geometric regularization of the Si_{12} framework upon insertion of a central metal impurity, which may act as electron donor or acceptor, is further documented by WSi_{12}, where the metal-Si charge transfer was found to be much stronger than in the case of $CuSi_{12}$ and the Si_{12} cage turned out to adopt the shape of a perfect hexagonal prism.[27,52]

We now turn to the details of the bonding in the substitutional isomer **12d** and the center-site isomer **12a**. Compared with the contribution of the atom 13Si in the HOMO of Si_{13} (C_{3v}), the Cu atom has a considerably larger *p* as well as small *d* components in the HOMO of **12d**. In addition, since the double chairs of **12d** are flatter than Si_{13} (C_{3v}) and the Cu-Si bond is shorter than the Si-Si bond [2.35 and 2.61 Å in **12d** and Si_{13} (C_{3v}), respectively], the Cu atom is closer to the upper chair and can interact not only with atoms in the upper chair, but also with the atoms in the lower chair. Figure 7(d) exhibits the HOMO of **12d** on the plane passing through Cu and the 1Si, 4Si, 7Si, and 10Si atoms. Obviously, Cu forms a relatively strong bond with the 1Si atom and a weaker bond with the 4Si-10Si bridge. For the interaction of Cu with the 3Si and 5Si atoms, and the 2Si-8Si and 6Si-12Si bridges, analogous observations are found. Here Cu shows a tendency to form multicenter bonds with as many as nine Si atoms in **12d**. This bonding behavior is quite different from that found in smaller $CuSi_n$ ($n=4,6,8,10$) clusters and also different from that in Si_{13} (C_{3v}), where the 13Si atom mainly interacts with the 2Si, 4Si, and 6Si atoms of the upper chair and forms no bonds with the atoms of the lower chair. This leads to the expectation that, if Cu is located at the center site, it would bond with all Si atoms of the double-chair framework and this would lead to a higher stability than **12d**. This structure is just **12a**.

In contrast to the substitutional isomer **12d**, the HOMO of the center-site isomer **12a** has no *s* or *p* contribution from the Cu atom, and its component of the Cu *d* character is also small. In fact, the interaction between Cu and the Si_{12} framework is weakly antibonding in the HOMO of **12a**.

A bonding interaction between Cu and the Si_{12} framework in **12a** is obvious from inspection of the second HOMO, which lies 0.87 eV below the HOMO. This orbital has strong *s* and *p* components on all Si atoms (30.9% Si *s* and 44.9% Si *p*) and 22.2% *p* character on the Cu atom which is almost twice as large as the contribution of Cu found in the HOMO of the substitutional structure **6b** (13.0% Cu *p*). As a result,

similar delocalized bonds are formed among all Si atoms of the upper and lower chairs [Fig. 7(d)], and the Cu atom interacts with all atoms of the double chairs through the overlap between the Cu p orbital and the delocalized orbitals of the double chairs [Fig. 7(d)], forming an overall delocalized bonding of the whole cluster. The contour maps in typical planes for the delocalized bond among all Si atoms in the upper chair (plane B) and the overall delocalized bond between Cu and the Si_{12} framework (plane A) are shown in Fig. 7(d). The delocalized bond in the lower chair is similar, but opposite in phase, to that of the upper chair. So the two chairs are not bound directly but are bound through the interaction with Cu. As the contribution of Cu to the second HOMO of **12a** is sizable and stems from the most diffuse p shell of Cu (see below), the overlap between the sp orbitals of the Si atoms and the p orbital of the Cu atom is effective and the role played by the second HOMO in the stabilization of the cluster is expected to be strong.

The natures of the bonding detected in **12a** and **12d** are quite different from all substitutional and adsorption structures we have discussed above for smaller $CuSi_n$ ($n=4,6,8,10$) clusters. These bonding differences can be related to the difference in the electronic configuration of Cu in these clusters. As seen from Table VI, the $4p$ population of Cu is usually quite small in the substitutional or adsorption structures of $CuSi_n$ clusters, and reaches a maximum of $0.07e$ in the substitutional structure **12d**. The $4p$ population of Cu becomes as large as $0.16e$ in the center-site structure **12a**. In addition, the $4d$ population of Cu in **12a** ($0.05e$) is also considerably larger than in **12d** and all other substitutional and adsorption structures of $CuSi_n$ clusters ($\leqslant 0.02e$). Therefore, the orbitals of Cu is the most diffuse in **12d** among all substitutional and adsorption structures of $CuSi_n$ clusters, and the orbitals of Cu in **12a** are even more diffuse than in **12d**. We have found that the $4p$ and $4d$ populations are considerably larger in all center-site structures than in the substitutional or adsorption structures of $CuSi_n$. For example, the electronic configuration of Cu in **10g** is $3d^{9.87}\,4s^{0.52}\,4p^{0.25}\,4d^{0.06}\,5s^{0.01}$ (Table VI). Thus it is a feature common to the cagelike isomers investigated here that the Cu atom at the center site tends to be diffuse and bond equally with all surrounding Si atoms, forming a characteristic multicenter bond.

IV. CONCLUSIONS

In this paper, a comprehensive study is reported on the geometric, energetic and bonding properties of $CuSi_n$ ($n=4,6,8,10,12$) clusters in the neutral and charged states using a hybrid density functional method (B3LYP) and the 6-311+$G(d)$ basis set. The results we have obtained can be summarized as follows.

(1) Three isomers for $CuSi_4$ and $CuSi_6$, nine isomers for $CuSi_8$, 20 isomers for $CuSi_{10}$, and 12 isomers for $CuSi_{12}$ are identified.

(2) The Si_n frameworks in most isomers of $CuSi_n$ are found to adopt the geometries of the ground-state or low-lying isomers of Si_n or Si_{n+1}, with Cu at various adsorption or substitutional sites, and the geometries of $CuSi_n$ can be classified into three types according to the position of Cu in the cluster: adsorption, substitutional and center-site geometries, with the substitutional type prevailing over the other two. In $CuSi_4$, $CuSi_6$, and $CuSi_8$, the Cu atom is found to occupy exclusively surface sites (adsorption or substitutional), whereas in $CuSi_{10}$ it is found at both surface and center sites with slight preference for the surface site. $CuSi_{12}$, however, stabilizes in a cagelike geometry. The most stable isomer of $CuSi_{12}$ adopts hexagonal double-chair structure with Cu at the center, which bears similarity to the structure of a regular hexagonal prism recently reported in Ref. 23 for WSi_{12}.

(3) The bulklike chair structure is not favorable for $CuSi_6$ and $CuSi_8$, but becomes the most stable form for $CuSi_{12}$, showing the onset of some bulklike behavior in $CuSi_{12}$.

(4) The influence of the positive and negative charges on the structures and energetics of all isomers of the $CuSi_n$ clusters studied was examined. The Cu atom acts as an electron donor in all $CuSi_n$ clusters. It is worth noting that the $3d$, $4d$, and $5d$ transition-metal (TM) atoms encaged in fullerenes are also found to exist as cations,[53] similar to the case of Cu in $CuSi_n$. However, the electron transfer in the endohedral metallofullerenes is much stronger than that found in $CuSi_n$ and the electrostatic interactions play a dominant role both in stabilizing the endohedral structures and in defining the metal impurity positions.[53]

(5) Various energetic properties, including binding and dissociation energies, adiabatic ionizational potentials and electron affinities, and vertical detachment energies are reported. The $CuSi_n$ and Si_n clusters show similar size dependence in their binding energies and adiabatic electron affinities, and different size dependencies in their adiabatic ionization potentials. The results for the binding and dissociation energies indicate that the Cu-Si interaction is much weaker than the Si-Si interaction. Therefore, the Si-Si interactions determine the structure of the Si_n framework in $CuSi_n$ and the stability of $CuSi_n$ can be well related to that of Si_n.

(6) The high abundance of $CuSi_{10}$ observed in Beck's mass spectrometric experiment is ascribed to the slightly enhanced stability of $CuSi_{10}$ and the existence of a multitude of nearly isoenergetic low-lying isomers.

(7) The bonding character in the representative isomers of neutral $CuSi_n$ is analyzed by comparison with bonding in Si_n^- or Si_{n+1}. The Cu-Si bond in $CuSi_n$ is quite strong for the substitutional and center-site structures, but weak for the adsorption structures where charge transfer and resulting ionic interaction are found to play a more important role. The bonding between Cu and the Si_n environment in the substitutional structures is found to be similar to that between the replaced Si atom and its surroundings within Si_{n+1}. The exception appears at the level of $CuSi_{12}$, where the Cu atom, both in the substitutional and in center-site structures, is found to form multicenter bonds with as many as nine (substitutional) to 12 (center-site) surrounding Si atoms.

In a continuation of the effort described here, it will be interesting to investigate the interaction of Si_n clusters with

other metal impurities, specifically $3d$ TM atoms along the lines investigated here. Our results on $CuSi_n$ could serve as reference in these research activities. Further, as the results presented here underscore the importance of hexagonal cage structures, a detailed comparison between the endohedral $CuSi_{12}$ unit identified in this work and the experimentally detected cagelike WSi_{12} cluster holds high interest.[27,52] This research has recently been finalized and will be reported elsewhere.[52]

ACKNOWLEDGMENT

The support given to this work by the National Science Foundation through the CREST program (HRD-9805465) is gratefully acknowledged.

*Email address: xiao@twister.jsums.edu
†Email address: hagx@twister.jsums.edu

[1] B. Kessler, A. Bringer, S. Cramm, Schlebusch, W. Eberhardt, S. Suzuki, Y. Achiba, F. Esch, M. Barnaba, and D. Cocco, Phys. Rev. Lett. **79**, 2289 (1997).
[2] A. N. Andriotis, M. Menon, and G. E. Froudakis, Phys. Rev. B **62**, 9867 (2000).
[3] W. Branz, I. M. L. Billas, N. Malinowski, F. Tast, M. Heinebrodt, and T. P. Martin, J. Chem. Phys. **109**, 3425 (1998).
[4] T. Guo, M. D. Diener, Y. Chai, M. J. Alford, R. E. Haufler, S. M. McClure, T. Ohno, J. H. Weaver, G. E. Scuseria, and R. E. Smalley, Science **257**, 1661 (1992).
[5] K. Raghavachari, J. Chem. Phys. **84**, 5672 (1986).
[6] K. Raghavachari and C. M. Rohlfing, J. Chem. Phys. **89**, 2219 (1988).
[7] K. Raghavachari and C. M. Rohlfing, J. Chem. Phys. **94**, 3670 (1991).
[8] A. Sieck, D. Porezag, Th. Frauenheim, M. R. Peterson, and K. Jackson, Phys. Rev. A **56**, 4890 (1997).
[9] A. A. Shvartsburg, B. Liu, M. F. Jarrold, and K. M. Ho, J. Chem. Phys. **112**, 4517 (2000).
[10] I. Rata, A. A. Shvartsburg, M. Horoi, Th. Frauenheim, K. W. M. Siu, and K. A. Jackson, Phys. Rev. Lett. **85**, 546 (2000).
[11] A. Hiraki, Surf. Sci. **168**, 74 (1986).
[12] A. A. Istratov and E. R. Weber, Appl. Phys. A: Mater. Sci. Process. **66**, 123 (1998).
[13] U. Wahl, A. Vantomme, G. Langouche, J. G. Correia, and ISOLDE Collaboration, Phys. Rev. Lett. **84**, 1495 (2000).
[14] A. Zunger and U. Lindefeldt, Phys. Rev. B **26**, 5989 (1982).
[15] F. Beeler, O. K. Andersen, and M. Scheffler, Phys. Rev. B **41**, 1603 (1990).
[16] D. E. Woon, D. S. Marynick, and S. K. Estreicher, Phys. Rev. B **45**, 13383 (1992).
[17] S. K. Estreicher, Phys. Rev. B **60**, 5375 (1999).
[18] S. M. Beck, J. Chem. Phys. **90**, 6306 (1989).
[19] J. J. Scherer, J. B. Paul, C. P. Collier, and R. J. Saykally, J. Chem. Phys. **102**, 5190 (1995).
[20] J. J. Scherer, J. B. Paul, C. P. Collier, and R. J. Saykally, J. Chem. Phys. **103**, 113 (1995).
[21] J. J. Scherer, J. B. Paul, C. P. Collier, A. O'Keefe, and R. J. Saykally, J. Chem. Phys. **103**, 9187 (1995).
[22] R. Kishi, S. Iwata, A. Nakajima, and K. Kaya, J. Chem. Phys. **107**, 3056 (1997).
[23] H. Hiura, T. Miyazaki, and T. Kanayama, Phys. Rev. Lett. **86**, 1733 (2001); Phys. News Update, No. 527, Feb. 2001.
[24] J. G. Han and Y. Y. Shi, Chem. Phys. **266**, 33 (2001).
[25] J. G. Han and F. Hagelberg, J. Mol. Struct.: THEOCHEM **549**, 165 (2001).
[26] J. G. Han and F. Hagelberg, Chem. Phys. **263**, 255 (2001).
[27] J. G. Han, C. Xiao, and F. Hagelberg, Struct. Chem. **13**, 173 (2002).
[28] C. Xiao and F. Hagelberg, J. Mol. Struct.: THEOCHEM **529**, 241 (2000).
[29] C. Xiao, F. Hagelberg, I. Ovcharenko, and W. A. Lester, Jr., J. Mol. Struct.: THEOCHEM **549**, 181 (2001).
[30] I. V. Ovcharenko, W. A. Lester, Jr., C. Xiao, and F. Hagelberg, J. Chem. Phys. **114**, 9028 (2001).
[31] K. Jackson and B. Nellermoe, Chem. Phys. Lett. **254**, 249 (1996).
[32] T. Nagano, K. Tsumuraya, H. Eguchi, and D. J. Singh, Phys. Rev. B **64**, 155403 (2001).
[33] Vijay Kumar and Yoshiyuki Kawazoe, Phys. Rev. Lett. **87**, 045503 (2001).
[34] Vijay Kumar and Yoshiyuki Kawazoe, Phys. Rev. B, **65** 073404 (2002).
[35] A. J. Wachter, J. Chem. Phys. **52**, 1033 (1970).
[36] L. A. Curtiss, P. W. Deutsch, and K. Raghavachari, J. Chem. Phys. **96**, 6868 (1992).
[37] P. Turski and M. Barysz, J. Chem. Phys. **111**, 2973 (1999).
[38] C. E. Moore, *Analysis of Optical Spectra*, NSRDES-NBS 34 (National Bureau of Standards, Washington, DC, 1971).
[39] H. Hotop and W. C. Lineberger, J. Phys. Chem. Ref. Data **4**, 539 (1975).
[40] P. Calaminici, A. M. Koster, N. Russo, and D. R. Salahub, J. Chem. Phys. **105**, 9546 (1996).
[41] L. A. Curtiss, K. Raghavachari, P. W. Deutsch and J. A. Pople, J. Chem. Phys. **95**, 2433 (1991).
[42] K. P. Huber and G. Herzberg, *Constants of Diatomic Molecules* (Van Nostrand Reinhold, New York, 1979)
[43] T. N. Kitsopoulos, C. J. Chick, Y. Zhao, and D. M. Neumark, J. Chem. Phys. **95**, 1441 (1991).
[44] A. Marijnissen and J. J. ter Meulen, Chem. Phys. Lett. **263**, 803 (1996).
[45] A. I. Boldyrev, J. Simons, J. J. Scherer, J. B. Paul, C. P. Collier, and R. J. Saykally, J. Chem. Phys. **108**, 5728 (1998).
[46] G. Riekert, P. Lamparter and S. Steeb, Z. Metallkd. **72**, 765 (1981).
[47] A. Luna, M. Alcami, O. Mo, and M. Yanez, Chem. Phys. Lett. **320**, 129 (2000).
[48] D. G. Leopold, J. Ho, and W. C. Lineberger, J. Chem. Phys. **86**, 1715 (1987).
[49] M. J. Frisch, G. W. Trucks, H. B. Schlegel, P. M. W. Gill, B. G. Johnson, M. A. Robb, J. R. Cheeseman, T. Keith, G. A. Petersson, J. A. Montgomery, K. Raghavachari, M. A. Al-Laham, V. G. Zakrzewski, J. V. Ortiz, J. B. Foresman, J. Cioslowski, B. B. Stefanov, A. Nanayakkara, M. Challacombe, C. Y. Peng, P. Y.

Ayala, W. Chen, M. W. Wong, J. L. Andres, E. S. Replogle, R. Gomperts, R. L. Martin, D. J. Fox, J. S. Binkley, D. J. Defrees, J. Baker, J. P. Stewart, M. Head-Gordon, C. Gonzalez, and J. A. Pople, GAUSSIAN 94, Revision E.3, Gaussian, Inc., Pittsburgh, PA, 1995.

[50] R. B. King, Z. Phys. D: At., Mol. Clusters **18**, 189 (1991).

[51] J. Lu, X. Zhang, X. Zhao, S. Nagase, and K. Kobayashi, Chem. Phys. Lett. **332**, 219 (2000).

[52] Frank Hagelberg, Chuanyun Xiao, and William A. Lester, Jr. (unpublished).

[53] D. P. Clougherty and F. G. Anderson, Phys. Rev. Lett. **80**, 3735 (1998).